



Chemical, electrochemical and photochemical catalytic oxidation of water to dioxygen with mononuclear ru complexes

Title	Chemical, electrochemical and photochemical catalytic oxidation of water to dioxygen with mononuclear ru complexes
Author(s)	Roeser, Stephen;Farràs, Pau;Bozoglian, Fernando;Martínez, Marta;Benet-Buchholz, Jordi;Llobet, Antoni
Publication Date	2011-01-27
Publisher	Wiley
Repository DOI	10.1002/cssc.201000358

Chemical, Electrochemical and Photochemical Catalytic Oxidation of Water to
Dioxygen with Mononuclear Ru Complexes

Stephan Roeser,^a Pau Farràs,^a Fernando Bozoglian,^a Marta Martínez,^a Jordi Benet-
Buchholz^a and Antoni Llobet^{a,b,*}

^aInstitute of Chemical Research of Catalonia (ICIQ), Av. Països Catalans 16, E-43007
Tarragona, Spain and ^bDepartament de Química, Universitat Autònoma de Barcelona,
Cerdanyola del Vallès, E-08193 Barcelona, Spain.

email: allobet@iciq.es

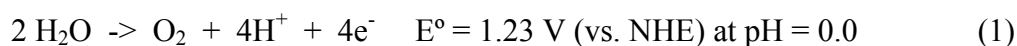
Abstract

Four new Ru^{II}-Cl and Ru^{II}-H₂O complexes containing the meridional 2,2':6',2''-terpyridine (trpy) ligand and the chelating 2-(5-phenyl-1H-pyrazol-3-yl)pyridine (H3p) ligand of general formula *in*- and *out*-[Ru^{II}(trpy)(H3p)(X)]ⁿ⁺ (X = Cl, n = 1; X = H₂O, n = 2) have been prepared, isolated and thoroughly characterized both in solution and in the solid state. In solution all the complexes have been characterized spectroscopically by UV-vis and NMR and their redox properties investigated by means of Cyclic Voltammetry, Square Wave Voltammetry and Coulometry techniques. In the solid state monocrystal X-ray diffraction analysis have been carried out for the *in* and *out* Ru-Cl complexes. The capacity of the Ru-aqua complexes to act as water oxidation catalysts (WOCs) has also been investigated chemically, electrochemically and photochemically. The performance of these complexes has also been compared to two previously described complexes of general formula *in*- and *out*-[Ru^{II}(trpy)(Hbpp)(H₂O)]²⁺ (Hbpp is 2,2'-(1H-pyrazole-3,5-diyl)dipyridine)), whose capacity as WOCs had not been previously described.

Keywords: water oxidation, redox catalysis, Ru complexes, redox properties

Introduction

The oxidation of water to molecular oxygen is a reaction that takes place in the dark at the OEC-PSII.¹ It is a very interesting reaction to be modeled from a bioinorganic perspective so as to gain insight into the mechanism that operates in this natural system. It is of still greater importance from an energetic perspective, since water oxidation is the key bottleneck currently associated with the development of commercial light harvesting devices for the photo-production of H₂ from water.² Water oxidation is a challenging task for a catalyst for two primary reasons: the first is the large endothermicity of the relevant reaction,



and the second is the significant molecular complexity from a mechanistic point of view, since two protons and two electrons have to be removed from each of two water molecules and an oxygen-oxygen bond formed between them. In spite of this, at the moment there is a significant number of molecular transition metal complexes that have shown activity with regard to the oxidation of water to oxygen,³ mainly based on Ru but also containing other metals such as Ir,⁴ Co,⁵ Fe,⁶ or Mn.⁷

Initially the design of molecular water oxidation catalysts (WOCs) based on well defined Ru complexes consisted on dinuclear Ru complexes containing two Ru-aqua groups inspired by the involvement of two water molecules indicated in equation (1).⁸ However, recently Meyer⁹ and Thummel¹⁰ showed that mononuclear complexes containing a single Ru-OH₂ group are also capable of behaving as a WOC. The above mentioned interests for this reaction together with the synthetic simplicity of preparing mononuclear as opposed to the complexity of preparing and purifying dinuclear or polynuclear complexes, has attracted new contributions to the field, that are providing exciting and valuable new insights.¹¹

While a significant number of efficient WOCs has now been described the number of mechanistic studies today remains very scarce due to the extraordinary complexity of this reaction.¹² It is worth mentioning a recent mechanistic endeavor by Meyer et al.¹³ that proposes the formation of metal hydroperoxidic intermediates that are generated

by a water nucleophilic attack (WNA) of a solvent molecule to a Ru=O group. The metal-hydroperoxide is then further oxidized to finally generate dioxygen. This mechanistic proposal is reminiscent of the one proposed for Cytochrome P-450 that catalyzes the reverse reaction namely the four electron reduction of dioxygen.¹⁴ Other mechanistic proposals find a bimolecular kinetic dependence on Ru=O and thus invoke the interaction of two Ru=O (I2M) to generate a peroxidic dinuclear intermediate that finally produces molecular oxygen.^{13,15}

In order to fully understand at a molecular level how the water oxidation takes place there is a need to generate a sufficiently large pool of WOCs so that the different parameters that influence the performance of the catalyst are identified and their effect understood. In this respect the role of the auxiliary ligand/s is fundamental to: a) influence the stability of higher oxidation states by electronic perturbations, b) to stabilize reaction intermediates, c) to exert geometrical distortions with constrained ligands that change the number of atoms coordinated to first coordination sphere, etc.

In order to further explore the chemistry of mononuclear Ru WOCs we have prepared and thoroughly characterized two new isomeric Ru-aqua *in-* and *out-* $[\text{Ru}^{\text{II}}(\text{trpy})(\text{H3p})(\text{H}_2\text{O})]^{2+}$ complexes containing the bidentate ligand H3p and the tridentate meridional trpy ligand (See Chart 1 for ligands drawing). Furthermore we have also explored the WO capacity of two related mononuclear Ru-aqua complexes *in-* and *out-* $[\text{Ru}^{\text{II}}(\text{trpy})(\text{Hbpp})(\text{H}_2\text{O})]^{2+}$ containing the Hbpp (see Chart 1) and trpy ligands whose synthesis and structure was reported previously but their capability as WOCs had not been investigated.¹⁶ Thus in the present paper we report the performance of 4 Ruthenium complexes as WOCs that constitute a family of catalysts with subtle variations in the electronic and geometric properties of the first coordination sphere of the Ru metal center.

Results

Synthesis and Structure and Spectroscopic Properties. The synthetic strategy followed to prepare the Ru complexes **1-2** is outlined in Scheme 1. $[\text{Ru}^{\text{II}}\text{Cl}_2(\text{DMSO})_4]$ is used as the starting material and then subsequently the H3p and then the trpy ligands are introduced in the coordination sphere of the Ru center to generate a mixture of $\text{Ru}^{\text{II}}\text{-Cl}$ isomeric complexes, *in-1*⁺ and *out-1*⁺ with 1:3 ratio respectively, in moderate yields. The isomers are then easily separated and purified through crystallization and by column chromatography in silica. Treatment of the pure $\text{Ru}^{\text{II}}\text{-Cl}$ complexes with Ag^+ generates the corresponding $\text{Ru}^{\text{II}}\text{-OH}_2$ complexes, *in-2*²⁺ and *out-2*²⁺, in excellent yields and with retention of the initial constitutional configuration. The *in/out* terminology is maintained here for the sake of consistency with related complexes **3** and **4** with the Hbpp ligand (see Scheme 1), that we have described previously.¹⁶ However the traditional *cis/trans* terminology could also be applied here taking into consideration the position of the Ru-Cl or Ru-OH₂ group with regard to the pyrazolylic group of the H3p or the Hbpp ligand respectively as shown in Scheme 2.

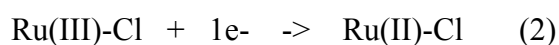
The structure of the Ru-Cl complexes, **1**(PF₆), in the solid state was elucidated via x-ray monocrystal diffraction analysis. Table 1 presents their crystallographic data whereas an Ortep view of their cationic moiety is displayed in Figure 1. Both Ru-Cl complexes present a distorted octahedral geometry where the trpy ligand acts in a meridional fashion, the H3p ligand in a chelating fashion and finally sixth coordination position is occupied by the chloro ligand. The bond distances and angles are unremarkable and thus similar to previous Ru complexes described in the literature.¹⁷ The most salient feature of the two structures is the hydrogen interaction between the Cl ligand and the pyrazolylic NH ($d_{\text{NH}} = 0.881 \text{ \AA}$, $d_{\text{HCl}} = 3.140 \text{ \AA}$, $d_{\text{NCl}} = 3.530 \text{ \AA}$, $\angle_{\text{NHCl}} = 109.28^\circ$) for *in-1*⁺ and the Cl ligand and the pyridylic CH ($d_{\text{CH}} = 0.950 \text{ \AA}$, $d_{\text{HCl}} = 2.727 \text{ \AA}$, $d_{\text{NCl}} = 3.341 \text{ \AA}$, $\angle_{\text{CHCl}} = 122.99^\circ$) for the *out-1*⁺ complex. The stronger H interaction for the *out* with regard to the *in*, is a consequence of the geometrical difference of 6-pyridyl vs. 5-pyrazolyl member rings involved as shown in Scheme 2. This H interaction in turn will be responsible for specific spectroscopic properties and differentiated reactivity as will be described below.

1D- and 2D-NMR spectroscopy for complexes **1-2** was carried in order to fully characterize them in solution, and their spectra are shown in Figure 2 and in the Supp. Inf. All resonances can be unambiguously characterized thanks to symmetry, integration and their 2D spectra, and demonstrate that the molecular structure obtained in the solid state is maintained in solution, as expected for inert low spin d^6 Ru(II) type of cations. The most interesting feature that can be observed when comparing the spectra of the two Cl isomers is the strong downfield shift of H14 for the case of the *out* isomer as a consequence of the stronger Cl \cdots H interaction discussed in the previous section.

The UV/Vis spectral features in dichloromethane or in aqueous solutions for the complexes described in this work are listed in the Experimental Section and in Table 2. The UV-vis spectra for *out-1*⁺ and *out-2*⁺ are presented in Figure 3 and for the rest of complexes are gathered at the Supp. Inf. Three main regions can be distinguished: one between 200 and 350 nm, in which very intense bands are observed due to intraligand $\pi-\pi^*$ transitions; another one between 350 and 550 nm, in which there are mainly broad unsymmetrical Ru($d\pi$)-trpy/bpp(π^*) metal-to-ligand charge transfer (MLCT) bands; and finally the region above 550 nm in which d-d transitions occur.¹⁸ At the MLCT region the Ru-Cl complex bands are clearly shifted to the red with regard to the Ru-H₂O complex due to the capacity of the anionic chloro ligand to destabilize $d\pi$ orbitals.¹⁹

Redox Properties. Electrochemical experiments were carried out by means of Cyclic Voltammetry (CV), Square Wave Voltammetry (SWV) and Coulometry.

For the Ru-Cl complexes **1**⁺ and **3**⁺ the experiments were carried out in organic solvents and all of them present chemically reversible and electrochemically quasireversible redox waves that are associated with their Ru(III)/Ru(II) couple.



From here on and for simplicity purposes, N-containing auxiliary ligands and charges on complexes are omitted in the equations in order to focus the attention at the site where the change is occurring.

In both cases the *in* isomers have lower redox potentials than the corresponding *out* isomers by 110 and 230 mV (see Table 2, entries 1-4). This is a feature that is also observed for the *cis*- and *trans*-[Ru(Cl)(pic)(trpy)]⁺ complexes as shown in entries 5-6 of the same Table. This effect can be rationalized in terms of H interactions and *trans* influence. As shown in Scheme 2 the *out/trans* complexes display stronger H interactions with the Cl ligand stabilizing the Ru(III) oxidation state and thus decreasing the Ru(III)/Ru(II) redox potential. On the other hand in the *out* and *trans* complexes the pyrazolyl and carboxyl donors respectively are situated *trans* with regard to the Ru-Cl bond. This allows a better transmission of sigma bonding electron density to the metal center than their corresponding *in/cis* isomers, a *trans influence*, resulting again in decrease of their corresponding redox potentials.

For the Ru-H₂O complexes **2**²⁺ and **4**²⁺ electrochemical experiments were performed at pH = 1.0 in 0.1 M triflic acid solutions. A representative example of the redox behavior of the aqua complexes is displayed in Figure 4 and the rest of the data is presented in the Supp. Inf. Furthermore a list of redox properties of complexes **1-4** is exhibited in Table 2 together with representative examples of related complexes previously described in the literature.²⁰

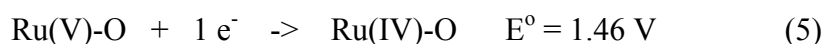
Figure 4A presents the electrochemical properties of complex *out*-**2**²⁺ as a representative example of this family of Ru-aqua complexes. As it can be observed in the CV a first chemically reversible and electrochemically quasireversible wave is observed that is associated with the III/II couple indicated below,



A redox titration presented as Supp. Inf. together with coulometry agree with the one electron nature assigned to this wave. A second chemically irreversible wave is also observed and is associated with the following process at pH = 1.0,



The E° in this case was calculated thanks to SWV. Further scanning to more positive potentials shows the presence of large anodic current that is associated with the formation of Ru(V) and the electrocatalytic oxidation of water to molecular oxygen,



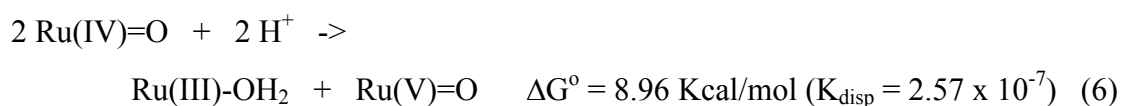
At this point the Ru(V)=O species is highly reactive and can generate dioxygen through a solvent water nucleophilic attack (WNA) to form a Ru-hydroperoxo species that ends up making O₂. The Ru(V)=O can also undergo a bimolecular process (I2M) to form a peroxo species that finally releases O₂.

It is important to see here that once the electrocatalytic process occur then two new cathodic waves appear at $E_{p,c} = 0.8 \text{ V}$ and $E_{p,c} = 0.4 \text{ V}$ with a decrease in intensity of the cathodic wave associated with the Ru(III)/Ru(II) couple of the *out-2*²⁺ complex, and thus manifests the existence of decomposition pathways competing with the electrocatalytic oxygen generation reaction.

A relatively similar redox behavior as the one described here for the *out-2*²⁺ is observed for the *out-4*²⁺ complex as shown in the Supp. Inf. For the cases of the *in-2*²⁺ the Ru(IV)/Ru(III) couple has much less intensity and in the case of the *in-4*²⁺ is practically not observed. However for the latter an electrocatalytic process associated with the generation of oxygen is seen at $E^\circ = 1.45 \text{ V}$ as is the case for the other Ru-aqua catalysts. The decrease in intensity of the Ru(IV)/Ru(III) redox couple, that involves electron transfer coupled to two protons, can be interpreted in terms of slow rate of heterogeneous electron transfer.²¹ Finally the variation of the Ru(III)-OH₂/Ru(II)-OH₂ redox potentials follows the same trend as in the case of the Ru-Cl complex in the sense that the *out/trans* complexes display roughly 40-115 mV lower potential than the corresponding *in/cis* complexes as can be seen in Table 4, entries 7-12.

Stability of Ru(IV) and Oxygen Generation. All the Ru(III)-OH₂ species derived from complexes **2** and **4** are stable for long periods of time at pH =1.0,

however their corresponding Ru(IV)=O are not stable at least within the time scale of the CV as indicated in the previous section. The stability of the Ru(IV)=O species from the *out-4*²⁺ was monitored by UV-vis spectroscopy and is displayed in Figure 5. Addition of one equivalent of [(NH₄)₂Ce(NO₃)₆] (Ce(IV)) to the Ru(III)-OH₂ species generates an intermediate that after a short period of time reverts to the initial Ru(III)-OH₂ species nearly quantitatively. This experiment can be repeated several times with small losses of the original Ru(III)-OH₂ species. Interestingly we found that the returning process was accompanied with the generation of molecular oxygen as shown in Figure 6. The Ru(IV)=O species can't be responsible for the generation of oxygen given the low redox potential for the IV/III couple as indicated in equation 3. Thus we assume that Ru(IV) disproportionates into Ru(V) and Ru(III),



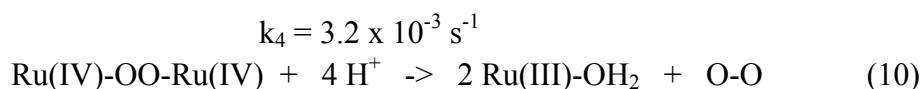
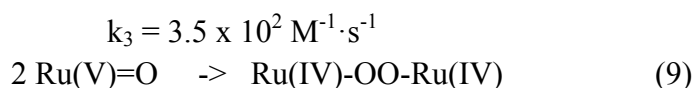
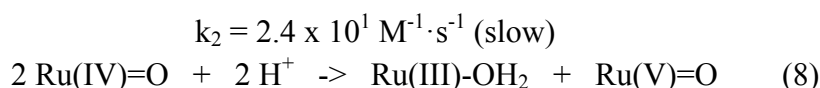
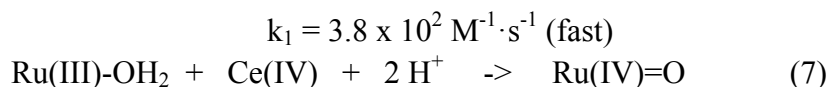
and then once formed the Ru(V) species oxidizes water to dioxygen. Even though the disproportionation reaction is highly disfavored thermodynamically the amount of Ru(III) and Ru(V) is not negligible. For instance an initial 2.5 mM solution of Ru(III) would produce a concentration of Ru(V) of 0.11 μM. The capacity of the Ru(V)=O to act as a WOC has been previously demonstrated in an electrocatalytic manner. The whole process is sketched in Scheme 3 where two different mechanisms for the critical O-O bond formation step, the WNA and the I2M, are indicated.

In order to obtain further insight into the whole process, kinetic analyses were carried out by means of UV-vis spectroscopy that are shown in Figure 5 and 6 and in the Supp. Inf. Data analyses were performed with Specfit²² that allowed to extract rate constants values for the different proposed processes, calculate spectra for the putative intermediates and generate species distribution diagrams.

Two cases were examined that contained two initial common reactions: a) a fast oxidation of Ru(III) to Ru(IV) (equation 7) and a second slower reaction involving the disproportionation of Ru(IV) into Ru(III) and Ru(V) (equation 8). At this point a number of reactions describing the reactivity of Ru(V) towards water (WNA mechanism) to

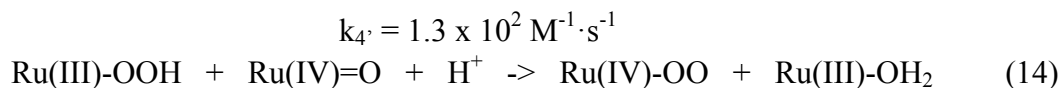
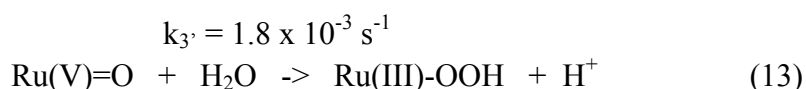
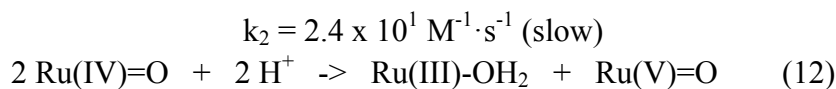
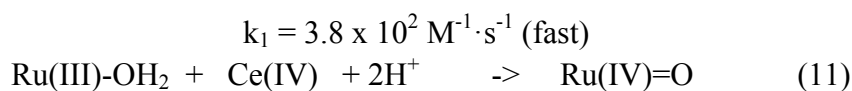
generate a Ru-hydroperoxide species (eq. 9) or towards coupling with itself to form a dinuclear peroxo bridge Ru complex (I2M mechanism; eq. 13) were considered.

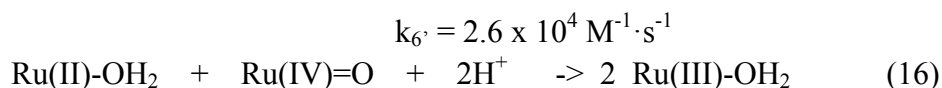
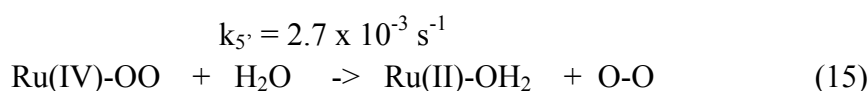
A) I2M Mechanism,



The symmetric bridging peroxo intermediate, Ru-OO-Ru, has been previously proposed in the case of the complexes containing the dinucleating ligand Hbpp²³ although at one unit lower oxidation state. Once this species are formed then the release of dioxygen constitutes the rate determining step for this mechanism (eq. 10).

B) WNA Mechanism,





The first two equations are common for the two mechanism involving the formation of the active Ru(V) following disproportionation of Ru(IV) (see eq. 11-12). Once formed the Ru(V) is proposed to undergo a water nucleophilic attack to generate the corresponding Ru(III)-OOH species (eq. 13), in an analogous manner as proposed recently for related mononuclear Ru complexes such as $[\text{Ru}(\text{trpy})(\text{bpm})(\text{H}_2\text{O})]^{2+}$ (bpm is 2,2'-bipyrimidine).¹³ At this point this species suffers a fast oxidation by the accumulated Ru(IV)=O species to generate Ru(IV)-OO species that are now responsible for the release of dioxygen (eq. 14 and 15) and the formation of Ru(II). The latter species are finally quickly oxidized to its original Ru(III) species (eq. 16).

Both mechanisms nicely match the data as can be seen in the fit of the inset in Figure 5 for the WNA and in the Supp. Inf. for the I2M. It is interesting to realize here that for both mechanisms the oxygen release is a slow process as shown in equation 10 and 15 for the I2M and WNA cases respectively. Related rate constants for the oxygen release process in the case of $[\text{Ru}(\text{trpy})(\text{bpm})(\text{H}_2\text{O})]^{2+}$ gives a value of $7.5 \times 10^{-4} \text{ s}^{-1}$ following a WNA mechanism.¹³ The critical O-O bond formation step in our case for the WNA is $k_3 = 1.8 \times 10^{-3} \text{ s}^{-1}$ (eq. 13) and is a bit slower than the one obtained for the previous complex that gives a value of $9.6 \times 10^{-3} \text{ s}^{-1}$. In this particular case the role of the highly electron withdrawing 2,2'-bipyrimidine ligand might be responsible for generating a more reactive Ru(V) oxidation state and manifests the important role of the auxiliary ligands in the water oxidation reactions. An I2M mechanism is invoked for the bipyrimidine complex at pH = 0.0 based on bimolecular Ru concentration dependence but quantitative values have not been reported yet and thus it can't be compared with our system.

It is also gratifying to state that the calculated oxygen evolution profile versus time (see Figure 6) following the two mechanisms proposed above nicely matches the

experimental one observed independently via Clark electrode in solution, especially for the WNA mechanism.

Chemically Induced Catalytic Oxidation of Water to Dioxygen. The aqua complexes 2^{2+} and 4^{2+} were tested with regard to their capacity to catalytically oxidize water to molecular oxygen upon addition of a strong oxidant such as Ce(IV). The gas evolution was monitored by both manometry and MS spectroscopy and the results are shown in Figure 7 and in the Supp. Inf. Molecular oxygen is the only gas generated in the catalytic process with Ru-aqua complexes 4^{2+} containing the Hbpp ligand. In sharp contrast for the case of the Ru-OH₂ complexes 2^{2+} containing the H3p ligand a mixture of O₂ and CO₂ is obtained with roughly a 5:1 ratio respectively.

As an example, for the case of *out*- 4^{2+} the system Cat 1 mM/Ce(IV) 100 mM/0.1 M triflic acid with a total volume of 1 mL at 25.0 °C gives 14 μmols of O₂ after 24 minutes that represent 14.0 TN and an efficiency of 56% with regard to the Ce(IV) oxidant. The initial rate of oxygen formation in this case is 52 nmols·s⁻¹. Under identical conditions the *in*- 4^{2+} gives only 8 TN (32% eff.) with a lower initial rate of 26 nmols·s⁻¹. These experiments manifest the superior behavior of the *out* isomer with regard to the *in* as a WOC.

For the case of the 2^{2+} complexes containing the H3p a similar trend is observed in the sense that the *out* isomer outperforms the *in*. For the particular case of *out*- 2^{2+} the system Cat 1 mM/Ce(IV) 100 mM/0.1 M triflic acid with a total volume of 2 mL at 25.0 °C gives 25.4 μmols of O₂ and 6.4 μmols of CO₂ after 24 minutes. This represents a TN of 12.7 for O₂ and 3.2 for CO₂, with initial rates of 45 and 9 nmols·s⁻¹ respectively. Under identical conditions the *in* isomer makes 10 TN of O₂ and 2.5 of CO₂ with rates of 4 and 1 nmols·s⁻¹ respectively.

Photochemically Induced Oxygen Evolution. The oxidation of water to dioxygen by complexes 2^{2+} and 4^{2+} was also carried out by photochemical means at pH = 7.0 in a phosphate buffer at 20.0 °C. For that purpose [Co^{III}(Cl)(NH₃)₅]²⁺ was used as a sacrificial electron acceptor and [Ru(bpy)₃]²⁺ as photosensitizer. A 150 W Xenon arc lamp with a 400 nm filter was used as a light source while the formation of

dioxygen was monitored with a Clark electrode in the gas phase. Scheme 4 shows the series of reactions that take place for the photochemical generation of O₂. In this scheme Ru_P represents [Ru^{II}(bpy)₃]²⁺ whereas Ru_C represent the WOC at low oxidation states. The term Ru_C stands for the Ru active species that is capable of carrying out oxidation of water to dioxygen and thus represents the four times oxidized Ru_C complex as indicated in the graph (x4).

Figure 7 shows the time profile of oxygen evolution for the Ru-aqua *out-2*²⁺, *out-4*²⁺, *in-4*²⁺ and [Ru^{II}(tpy)(bpy)(H₂O)]²⁺ (bpy is the bidentate chelating ligand 2,2'-bipyridine), the latter was also tested for comparison purposes. All these complexes are capable of performing the photochemically induced oxidation of water to dioxygen with the following degree of activity *in-4*²⁺ > *out-2*²⁺ > [Ru^{II}(tpy)(bpy)(H₂O)]²⁺ > *out-4*²⁺. In the best case the *in-4*²⁺ complex is capable of generating 1.4 μmols of O₂ that represents a modest TN of 4 after the blank subtraction with Ru_P and no WOC. The relative reactivity of the complexes shown here is radically different from the one reported in solution. This can be due to the fact that the photochemical experiments are carried out at pH = 7.0 whereas the chemical oxidations have been performed at pH = 1.0.

Discussion

During the last two years a significant number of polynuclear²⁴ as well as mononuclear Ru-aqua complexes have been reported in the literature²⁵ that are capable of oxidizing water to molecular oxygen. A variety of auxiliary ligands have been used to complete the Ru coordination sphere including: a) neutral or anionic, b) N-based or O-based, c) monodentate, bidentate and/or tridentate, etc. The performance of these WOCs has been shown to be largely dependent on the nature of the rest of the auxiliary ligands. Therefore it is important to understand the role of the auxiliary ligands to be able to design efficient and effective WOCs.

Electronic and Geometrical Influences Induced by Auxiliary Ligands. The family of 4 Ru-aqua complexes described here, *in-*, *out-2*²⁺ and *in-*, *out-4*²⁺, have been chosen to try to understand how electronic, steric and geometric factors influence the performance of the Ru WOC. All these complexes contain a common Ru-aqua group,

a meridional trpy ligand and are differentiated by having Hbpp or H3p ligands. The latter share a common non-symmetric environment, that is a N-N' chelating ligand that is composed of pyridyl and a pyrazole groups and they are differentiated by the non coordinated pending group that is a pyridyl in the case of Hbpp and an phenyl in the case of the H3p.

Due to the meridional nature of trpy, the non-symmetric Hbpp or H3p ligands can be coordinated in two different manners that are termed *in* and *out* and where the pyrazole moiety is coordinated *cis* or *trans* to the Ru-OH₂ bond (see Scheme 2). Since the 5 member pyrazole group is better σ -donor and a worse π -acceptor than the pyridyl group this results in a significantly stronger *trans* influence in the *out/trans* isomers than their corresponding *in/cis* isomers. This in turn results in a lowering of redox potentials for the former versus the latter. Furthermore the geometrical differences of the 5 member pyrazole ring with regard to the six member pyridyl rings results in a much stronger H-bonding for the *out/trans* isomers than for the *in/cis*. This H-interaction is beautifully observed in the NMR spectra as shown in Figure 2. The stronger H-interaction also allows stabilizing higher oxidation states as has been shown for related Fe and Mn complexes.²⁶ In this particular case it is interesting to note that the first oxidation process, from Ru(II) to Ru(III) at pH = 1.0 involves a single electron transfer but the next oxidation involves losing two protons and one electron from Ru(III) to Ru(IV) as exemplified in eq. 3 and 4. Thus the involvement of PCET allows keeping the thermodynamic potentials relatively low with also narrow differences between E°(IV/III) and E°(III/II). The next oxidation from Ru(IV) to Ru(V) involves a single OSET process and thus does not benefit from the stabilizing effect of PCET. In related complexes suffering OSET process, such as the [Ru(bpea)Cl₃] complex, the difference between the IV/II and III/II redox potential is close to 1 V.²⁷ In the *out-2*²⁺ and *out-4*²⁺ the differences between the V/IV vs. IV/III are much lower than in the preceding example and are of the order of less than 500 mV. This E° lowering of higher oxidation states can be attributed to the stabilizing effect of the hydrogen interaction.

Dioxigen Generation and Deactivation Pathways. The thermodynamic redox potential for the Ru(IV)/Ru(III) couple (eq. 4) is too low to oxidize water and

thus it is essential to reach higher oxidation states if it has to act as a WOC. Thus we propose that once generated the Ru(IV) oxidation state deactivates to the original Ru(III) and O₂ through a disproportion reaction as indicated in eq. 8, that generates Ru(III) and Ru(V). Even though this reaction is highly disfavored from a thermodynamic point of view, once generated the Ru(V) can react via one of the two pathways, I2M or WNA (Scheme 3) to finally make O₂, as we have experimentally shown, and that constitutes the driving force for the whole sequence of reactions. Based on kinetic grounds both mechanisms can fit the data although it is impressive to see how well the WNA mechanism can fit the experimental generation of O₂. In the present case further kinetic analysis should be carried out to be able to discern between the two possible mechanisms although both of them might be occurring at the same with a different extent. Evidence for the operation of one mechanism or the other has been previously found in the literature for the [Ru(trpy)(bpm)(H₂O)]²⁺ complex simply changing the pH from 0.0 to 1.0,¹³ and puts forward how small changes in the system can generate dramatic differences in reactivity.

Under excess of Ce(IV) it is exciting to see that all four Ru-aqua complexes, **2**²⁺ and **4**⁴⁺, are capable of acting as WOCs and generate copious amounts of dioxygen. However it is interesting to see that for the cases of complexes **2**²⁺ containing the H3p ligand, dioxygen is accompanied with the formation of CO₂ in a 5:1 ratio respectively whereas in sharp contrast for the ones containing the Hbpp ligand not even traces of CO₂ are found. This differentiated reactivity clearly points out that the initial oxidation site of the complex is the phenyl group. In the case of complexes containing Hbpp the non-coordinated pyridyl group at this pH is protonated and this might protect it from a quick oxidation as opposed to the phenyl ring of the complexes containing the H3p ligand. For the latter a plausible oxidation process might involve the formation of phenol group that then is quickly oxidized to quinone, followed by a sequence of reactions that finally leads to the formation of CO₂. The oxidation of benzene to phenol under mild conditions is actually one of the most challenging reactions faced by today's chemical industries.²⁸ These results thus put forward the fact that a catalyst capable of oxidizing water to O₂ will also be a powerful catalyst for the oxidation of many organic substrates. It also manifests how carefully, the auxiliary ligands should be chosen, so that bimolecular deactivation is eradicated. It is also interesting to observe that the *out* isomers always outperform the

in ones a phenomenon that can be associated with the higher capacity of the *out* isomer to form H-interactions with the intermediates species and thus lower its accessibility. This *in/out* differentiated reactivity manifests once more the importance of the auxiliary ligands in dictating the nature of the active species that in turn influence the potential reaction pathways obeyed.

Finally in the present work we show how the WOC can be performed chemically, electrochemically or photochemically. In the latter case several reactions have to work in harmony so that the whole process can achieve the final goal as shown in Scheme 3. Even though we have shown the viability of the concept it is obvious that the whole device is in need of improvement since the TN (turnover number) achieved under these conditions is about a third with regard of using a simple chemical oxidation. This is an indication of the increased complexity of the system under photochemically induced conditions, has also been obtained for related system previously described in the literature and is generally ascribed to photocatalyst degradation due to competing pathways after photoexcitation.²⁹ The latter can be avoided or minimized when the oxidized photosensitizer Ru_P reacts very fast with the Ru_C catalyst as is the case for instance of the Ru-POM (POM is a polyoxometalate anionic ligand) systems recently described by Bonchio et al. Further work is in progress in our laboratories headed at optimizing these systems exploring the influence of parameters such as pH, nature of the photosensitizer, nature of sacrificial electron acceptor, etc.

Acknowledgements

Support from SOLAR-H2 (EU 212508) and MICINN (CTQ2010-21497 and Consolider Ingenio 2010 CSD2006-0003) are gratefully acknowledged. SR is grateful for the award of doctoral grant from MICINN.

Supporting Information. CIF files, together with further spectroscopic (1D and 2D NMR, and MS), electrochemical and kinetic characterization for the reported complexes. This material is available free of charge via Internet at <http://pubs.acs.org>. The supplementary crystallographic data can also be obtained free of charge via www.ccdc.cam.ac.uk/conts/retrieving.html (or from the Cambridge Crystallographic

Data Centre, 12, Union Road, Cambridge CB2 1EZ, U.K.; fax +44 1223 336033 or E-mail: deposit@ccdc.cam.ac.uk).

Experimental Section:

Materials. Trifluoromethanesulfonic acid (99+%) was purchased from STREM/CYMIT. All other reagents used in this work were obtained from Aldrich Chemical Co. in the highest commercially available grade and were used without further purification. Reagent grade organic solvents were obtained from SDS. MeOH was freshly distilled over Mg/I₂ before use. Highly pure water was obtained by passing it through an UltraClear water purifier system from SG Wasseraufbereitung und Regenerierstation GmbH (Conductivity at 25 °C = 0.055 μS/cm), followed by distillation over MnO₄⁻ to remove any possible organic impurities.

Preparations. [Ru(Cl)₂(DMSO)₄]³⁰ and the H3p³¹ ligand were prepared according to literature procedures. Complexes *in*- and *out*-[Ru(Cl)(Hbpp)(trpy)]⁺, *in*- and *out*-**3**⁺, and *in*- and *out*-[Ru(H₂O)(Hbpp)(trpy)]²⁺, *in*- and *out*-**4**²⁺, were prepared via a previously published procedure.¹⁶ All synthetic manipulations were routinely performed under argon atmosphere using Schlenck techniques.

***in*- and *out*-[Ru(Cl)(H3p)(trpy)](PF₆)·1.5H₂O, *in*- and *out*-**1**(PF₆)·1.5H₂O.** A sample of 441 mg (0.91 mmol) of [Ru(Cl)₂(DMSO)₄] and 201 mg (0.91 mmol) (H3p) were dissolved in 150 mL of methanol. The yellow suspension was heated to reflux for 18 h. After cooling down to RT, 212 mg (0.91 mmol) of 2,2':6',6''-terpyridine are added to the yellow suspension and anew heated to reflux overnight. The dark reaction mixture was reduced to dryness and the solid obtained was dissolved in 10 mL of a 30:1 mixture of MeOH:NH₄OH (28% in water). A purple precipitate **P1** is filtered off and washed two times with 5 mL of the same MeOH:NH₄OH solution. The filtrate solution **F1**, which contains mainly the *in*-isomer, is purified by column-chromatography, *vide infra*. The purple solid **P1** is dissolved in 10 mL of a MeOH:HCl_(conc.) solution 10000:1 and 1 mL of a saturated aqueous NH₄PF₆ solution is added. Afterwards 100 mL of water are added under vigorous stirring. The fine suspension that is generated immediately is left in the fridge over night. The precipitate obtained is filtered off, washed twice with 5 mL of water and 10 mL of

diethylether and dried in vacuum. A sample of 302 mg (45 %) of the **out-1(PF₆) 1.5H₂O** isomer is obtained. Elemental analysis, Calcd. (%) for (C₂₉H₂₂ClF₆N₆PRu·1.5H₂O): C, 45.7; H, 3.3; N, 11.0. Found: C, 45.6; H, 3.1; N, 11.0. ¹H NMR (d₆-DMSO): δ (ppm) 9.96 (d, ³J₁₋₂ = 5.6 Hz, 1H, H1), 8.77 (d, ³J₂₁₋₂₂ = ³J₂₃₋₂₂ = 7.6 Hz, 2H, H21, H23), 8.67 (d, ³J₁₈₋₁₇ = ³J₂₆₋₂₇ = 7.6 Hz, 2H, H18, H26), 8.50 (d, ³J₄₋₃ = 7.6 Hz, 1H, H4), 8.32 (t, ³J_{3-2,4} = 7.6 Hz, 1H, H3), 8.18 (t, ³J_{22-23,21} = 7.6 Hz, 1H, H22), 7.97 (t, ³J_{17-18,16} = ³J_{27-28,26} = 7.6 Hz, 2H, H17, H27), 7.89 (t, ³J_{2-1,3} = 6.6 Hz, 1H, H2), 7.71 (s, 1H, H7), 7.64 (d, ³J₁₅₋₁₆ = ³J₂₉₋₂₈ = 5.6 Hz, 2H, H15, H29), 7.45 (d, ³J₁₄₋₁₃ = ³J₁₀₋₁₁ = 7.2 Hz, 2H, H10, H14), 7.40 (m, 5H, H11, H12, H13, H16, H18). ¹³C NMR (d₆-DMSO): δ (ppm) 159.6 (C19, C25), 159.4 (C1), 153.7 (C6), 152.5 (C15, C29), 146.9 (C8), 137.2 (C3, C17, C27), 134.1 (C22), 129.5 and 127.7 (C9, C11, C12, C13, C16, C28), 126.5 (C14, C10), 125.1 (C2), 123.6 (C18, C26), 122.5 (C4, C21, C23), 102.8 (C7). NMR assignments for all complexes are keyed in Figure 1. MS (pyrene/MeOH): *m/z* 590.0 (M – HPF₆)⁺, 555.5 (M – HCIPF₆)⁺. UV-Vis (CH₂Cl₂): λ_{max}, nm (ε, M⁻¹cm⁻¹) 241 (47010), 277 (37720), 282 (37790), 323 (34440), 413 (7100), 502 (8210), 600 (1520), 657 (1435). Echem vs. SSCE in DCM containing 0.1 M TBAH: E_{1/2}^{III/II} = 0.69 V, ΔE = 60 mV.

A column chromatography (30 cm long, 2 cm width) under silica (70-200 μm) is carried out with the, to 5 mL volume reduced, filtrate **F1** using MeOH:NH₄OH 30:1 as eluent. The first orange fraction is discarded and contains Ru(trpy)₂²⁺. A second purple fraction contains a small amount of the **out-1**⁺ isomer. Then a third brownish fraction is eluted with MeOH:HCl(conc.) 10000:1 that contains the **in-1**⁺ isomer. The volume of the latter fraction is reduced to 10 mL and then 1 mL of saturated aqueous NH₄PF₆ solution is added. Finally under vigorous stirring 100 mL of water are added and the flask left overnight in the fridge. The fine crystalline precipitate is filtered off, washed twice with 10 mL of water and 10 mL of diethylether, After drying in vacuum a sample of 101 mg (15 %) of **in-1(PF₆) 1.5H₂O** are obtained. Elemental analysis, Calcd. (%) for (C₂₉H₂₂ClF₆N₆PRu·1.5H₂O): C, 45.7; H, 3.3; N, 11.0. Found: C, 45.4; H, 3.1; N, 11.1. ¹H NMR (d₆-acetone): δ (ppm) 8.73 (d, ³J₂₁₋₂₂ = ³J₂₃₋₂₂ = 8.2 Hz, 2H, H21, H23); 8.61 (d, ³J₁₈₋₁₇ = ³J₂₆₋₂₇ = 8.2 Hz, 2H, H18, H26); 8.24 (d, ³J₄₋₃ = 8.2 Hz, 1H, H4); 8.2 (m, 3H, H10, H14, H22); 8.09 (d, ³J₁₅₋₁₆ = ³J₂₉₋₂₈ = 5.4 Hz, 2H, H15, H29); 8.05 (s, 1H, H7); 8.00 (t, ³J_{17-16,18} = ³J_{27-26,28} = 7.8 Hz, 2H, H17, H27); 7.77 (t,

$^3J_{3-2,4} = 7.8$ Hz, 1H, H3); 7.64 (t, $^3J_{13-12,14} = ^3J_{11-10,12} = 7.7$ Hz, 2H, H11, H13); 7.56 (t, $^3J_{12-10,11} = 7.7$ Hz, 1H, H12); 7.46 (d, $^3J_{16-15,17} = ^3J_{28-27,29} = 6.6$ Hz, 2H, H16, H28); 7.39 (d, $^3J_{1-2} = 5.9$ Hz, 1H, H1); 6.98 (t, $^3J_{2-1,3} = 6.6$ Hz, 1H, H2). ^{13}C NMR (d_6 -acetone): δ (ppm) 159.2 (C9, C20, C24), 158.9 (C19, C25), 153.2 (C15, C29), 152.0 (C1), 151.4, 149.3 (C6, C8), 136.8 (C17, C27), 135.8 (C3), 133.2 (C22), 129.6 (C12), 129.3 (C13, C11), 127.3 (C16, C28), 126.4 (C10, C14), 124.4 (C2), 123.3 (C18, C26), 122.4 (C21, C23), 122.0 (C4), 102.5 (C7). MS (pyrene/MeOH): m/z 590.0 ($\text{M} - \text{HPF}_6$)⁺, 555.5 ($\text{M} - \text{HCIPF}_6$)⁺. UV-Vis (CH_2Cl_2): λ_{max} , nm (ϵ , $\text{M}^{-1}\text{cm}^{-1}$) 240 (40210), 276 (33830), 282 (33150), 318 (33440), 419 (6330), 487 (7440), 513 (7210), 594 (1450), 670 (750). Echem vs. SSCE in DCM containing 0.1 M TBAH: $E_{1/2}^{\text{III/II}} = 0.81$ V, $\Delta E = 60$ mV.

***out*-[Ru(3p)(trpy)(H₂O)](ClO₄), *out*-[2(-H⁺)](ClO₄).** A sample of 100 mg (0.136mmol) of *out*-1(PF₆) and 23.1 mg (0.163mmol) of AgNO₃ are dissolved in 50 mL of degassed Acetone/H₂O (3:1) and refluxed for 4 h in the absence of light. A fine precipitate of AgCl is filtered through Celite. Then 2 mL of a saturated solution of NaClO₄ are added to the filtrate followed by a reduction of the volume till a solid appears. The solid is filtered off, washed with a minimum amount of H₂O and Et₂O and dried in vacuum to give a black solid. A column chromatography (30 cm long, 2 cm width) under basic alumina (Brockmann I, standard grade) is carried out to purify the crude product, using DCM:MeOH 50:1 as eluent. A black fraction is collected that upon adding 1 mL of a saturated solution of NaClO₄ generates a black solid that is filtered washed with H₂O and Et₂O consecutively and dried in vacuum. Yield = 20 mg (29.9 mmol) (22 %) of *out*-[2(-H⁺)](ClO₄). Elemental analysis, Calcd. (%) for (C₂₉H₂₃ClN₆O₅Ru): C, 51.8; H, 3.5; N, 12.5. Found: C, 52.1; H, 3.6; N, 12.3. MS (MeOH): m/z 587.1 ($\text{M} - (\text{H}_2\text{O} + \text{ClO}_4) + \text{CH}_3\text{OH}$), 573.1 ($\text{M} - \text{ClO}_4$), 555.1 ($\text{M} - (\text{H}_2\text{O} + \text{ClO}_4)$). UV-Vis ($\text{CF}_3\text{SO}_3\text{H}$, pH = 1.0): λ_{max} , nm (ϵ , $\text{M}^{-1}\text{cm}^{-1}$) 273 (39000), 279 (39600), 316 (35200), 390 (6600), 475 (7400). Echem (vs. SSCE): $E_{1/2}^{\text{III/II}} = 0.97$ V, $\Delta E = 100$ mV (DCM-TBAH (0.1M)); $E_{1/2}^{\text{III/II}} = 0.30$ V, $\Delta E = 100$ mV (DCM-TBAH (0.1M)); At pH = 1.0 $\text{CF}_3\text{SO}_3\text{H}$: $E_{1/2}^{\text{III/II}} = 0.67$ V ($\Delta E = 60$ mV), $E_{\text{p,c}}^{\text{IV/III}} = 1.09$ V.

***in*-[Ru(3p)(trpy)(H₂O)](PF₆)·H₂O, *in*-[2(-H⁺)](PF₆)·H₂O.** This complex was obtained in the same manner as *out*-[2(-H⁺)]⁺, but using NH₄PF_{6(aq.,sat.)} instead of

NaClO_{4(aq.,sat.)}. Yield = 23 mg, (27.2 mmol) (20%). Elemental analysis, Calcd. (%) for (C₂₉H₂₄F₁₂N₆OP₂Ru·H₂O): C, 39.5; H, 3.0; N, 9.5. Found: C, 39.3; H, 3.1; N, 9.3. MS (MeOH): *m/z* 587.2 (M – (H₃O + 2PF₆) + CH₃OH)⁺, 572,2 (M – H₂P₂F₁₂)⁺. UV-Vis (CF₃SO₃H, pH = 1.0): λ_{max}, nm (ε, M⁻¹cm⁻¹) 273 (34300), 279 (34700), 314 (33700), 392 (5200), 460 (7100). Echem vs. SSCE: E_{1/2}^{III/II} = 1.10 V (ΔE = 100 mV) in 0.1 M TBAH in DCM; E_{1/2}^{III/II} = 0.74 V (ΔE = 60 mV) and E_{p,c}^{IV/III} = 1.09 V at pH = 1.0 in 0.1 M CF₃SO₃H.

Instrumentation and Measurements. UV-Vis spectroscopy was performed either on a Cary 50 (Varian) UV-Vis spectrophotometer in 1 cm quartz cuvettes or a TidasII (J&M Instruments). Cyclic Voltammetry (CV) and Square Wave Voltammetry (SWV) experiments were performed on an IJ-Cambria HI-660 potentiostat using a three-electrode cell. Typical CV experiments were carried out at a scan rate of 50 mV/s. SWV experiments were performed with the following parameters: Step E = 2 mV, SW Amplitude = 25 mV, SW Frequency = 15 Hz and Sensitivity = 1·10⁻⁵ A/V. A glassy carbon electrode (2 mm diameter) was used as working electrode, platinum wire as auxiliary electrode, and a SSCE as a reference electrode. Working electrodes were polished with 0.05 micron Alumina paste and washed with distilled water and acetone followed by blow-drying, before each measurement. All cyclic voltammograms presented in this work were recorded in the absence of light and inside a Faradaic cage. The complexes were dissolved either in CH₂Cl₂ (DCM) containing the necessary amount of n-Bu₄NPF₆ (TBAH) as supporting electrolyte to yield a 0.1 M ionic strength solution. In aqueous solution the electrochemical experiments were carried out in 0.1 M CF₃SO₃H (pH = 1.0). E_{1/2} values reported in this work were estimated from CV experiments as the average of the oxidative and reductive peak potentials (E_{p,a} + E_{p,c})/2 or taken as E(I_{max}) from SWV measurements. The NMR spectroscopy experiments were performed on a BrukerAvance 400 Ultrashield NMR spectrometer. Samples were run in d₆-DMSO or d₆-acetone with internal references (residual protons). Elemental analysis was performed using an EA-1108, CHNS-O elemental analyzer from Fisons Instruments. Manometric measurements were performed with homemade water-jacked glass reactor coupled to a Testo 521 manometer. Composition of the gaseous phase was determined by online mass-spectrometry with an OmniStarTM GSD 301 C (Pfeiffer) quadrupol mass-

spectrometer. Oxygen generation in solution was measured via a water-jacket Clark-electrode reactor from Hansatech. In a typical experiment, 1 mL of a 2 mM complex solution in $\text{CF}_3\text{SO}_3\text{H}$ ($\text{pH} = 1.0$) was degassed with argon until no oxygen could be detected. The reactor was then closed with a septum sealed adapter that excluded the gas phase. A minimum volume of previously degassed Ce(IV) solution, was then added directly into the reaction solution with a Hamilton syringe. Blanc experiments were performed by addition of Ce(IV) solution to neat $\text{CF}_3\text{SO}_3\text{H}$ ($\text{pH} = 1.0$) in the absence of catalyst. Spectroelectrochemical measurements were performed in a homemade three compartment bulk electrolysis cell, with platinum grid as working electrode, Pt wire as counter electrode and a SSCE reference electrode. An optical probe (10 mm optical path length) from Hellma was introduced to follow the electrolysis spectroscopically. Chemical redox spectrophotometric titrations were performed by sequential addition of a small volume of $(\text{NH}_4)_2[\text{Ce}^{\text{IV}}(\text{NO}_3)_6]$ solution in $\text{CF}_3\text{SO}_3\text{H}$ ($\text{pH} = 1.0$) ($20 \mu\text{L}/\text{redox equivalent}$) to the complex solution (3 mL) in standard 1 cm Quartz cuvettes.

Kinetics. Experiments were performed on a Cary 50 spectrophotometer equipped with a temperature controlled cell holder. The cell holder was constantly purged with nitrogen to avoid condensation of air humidity. In a typical experiment, to a 3 mL solution of *out-4*²⁺ ($1 \cdot 10^{-4}$ M) in 0.1 M $\text{CF}_3\text{SO}_3\text{H}$, 2 eq. of Ce^{4+} in $20 \mu\text{L}$ $\text{CF}_3\text{SO}_3\text{H}$ ($\text{pH} = 1.0$) were added at $5 \text{ }^\circ\text{C} \pm 0.1 \text{ }^\circ\text{C}$. First and second order rate constants were calculated by global fitting method using Specfit.

Photochemical oxygen evolution. Irradiation was carried out with a 150 W Xenon arc lamp equipped with a 400 nm cutoff filter to remove UV and IR radiation. The intensity of the radiation was approximately $0.3 \text{ W}/\text{cm}^2$. The temperature of the cell was maintained constant at 20°C thanks to water circulation through a jacketed compartment attached to the main cell. Oxygen evolution was analyzed with a gas-phase Clark-type oxygen electrode (Unisense Ox-N needle microsensor). The electrode was calibrated using nitrogen saturated, air saturated and a known amount of oxygen within the range of concentrations obtained in our experiments. The photochemical experiments involved a three component system: catalyst, sensitizer and sacrificial electron acceptor dissolved in 5 mL of a 50 mM phosphate buffer

solution (pH = 7.04). A typical experiment involved degassing, the above mentioned solution, and dissolving Catalyst, $[\text{Ru}(\text{bpy})_3]^{2+}$ and $[\text{Co}(\text{NH}_3)_5\text{Cl}]^{2+}$ with concentration of $8.0 \cdot 10^{-5}$ M, $1.1 \cdot 10^{-3}$ M, and $4.8 \cdot 10^{-2}$ M, respectively.

X-ray Structure Determination. Suitable crystals of *out-1*(PF₆) and *in-1*(PF₆) were grown as brown cubes, from slow diffusion of diethylether into an acetone solution of the complex. The measured crystals were prepared under inert conditions immersed in perfluoropolyether as protecting oil for manipulation. Data collection were made on a Bruker-Nonius diffractometer equipped with an APEX 2 4K CCD area detector, a FR591 rotating anode with MoK_α radiation, Montel mirrors as monochromator and a Kryoflex low temperature device ($T = -173$ °C). Full-sphere data collection was used with ω and φ scans. *Programs used:* Data collection APEX-2³², data reduction Bruker Saint³³ V/.60A and absorption correction SADABS³⁴. Structure Solution and Refinement were carried out using the SHELXTL³⁵ program. The crystal data parameters are listed in Table 2. The asymmetric unit of *out-1*(PF₆) is made up of the cationic unit containing the Ru metal and the PF₆ anionic unit that is disordered in two positions with a ratio 60:40. Further an acetone and a water molecule are also disordered in three positions with a ratio (60:28:12) and two positions with a ratio of 60:40 respectively. The asymmetric unit of *in-1*(PF₆) is made up of a cationic subunit containing the Ru metal, one disordered PF₆ anion (rotational disorder) and a disordered position with 75 % of acetone and 25 % of diethylether.

References

1 (a) J. Yano, J. Kern, K. Sauer, M. J. Latimer, Y. Pushkar, J. Biesiadka, B. Loll, W. Saenger, J. Messinger, A. Zouni, V. K. Yachandra, *Science* **2006**, *314*, 821-825 ; (b) M. Haumann, P. Liebisch, C. Müller, M. Barra, M. Grabolle, H. Dau, *Science* **2005**, *310*, 1019-1021.

² V. Balzani, A. Credi, M. Ventura, *Chem. Sus. Chem.* **2008**, *1*, 26-58.

³ X. Sala, M. Rodriguez, I. Romero, L. Escriche, A. Llobet, *Angew. Chem. Int. Ed.* **2009**, *48*, 2842-2852.

-
- ⁴ (a) J. F. Hull, D. Balcells, J. D. Blakemore, C. D. Incarvito, O. Eisenstein, G. W. Brudvig, R. H. Crabtree, *J. Am. Chem. Soc.* **2009**, *131*, 8730–8731; (b) N. D. McDaniel, F. J. Coughlin, L. L. Tinker, S. Bernhard, *J. Am. Chem. Soc.* **2008**, *130*, 210–217.
- ⁵ (a) M. Risch, V. Khare, I. Zaharieva, L. Gerencser, P. Chernev, H. Dau, *J. Am. Chem. Soc.* **2009**, *131*, 6936–6937; (b) Q. Yin, J. M. Tan, C. Besson, Y. V. Geletii, D. G. Musaev, A. E. Kuznetsov, Z. Luo, K. I. Hardcastle, C. L. Hill, *Science* **2010**, *328*, 342–345.
- ⁶ W. C. Ellis, N. D. McDaniel, S. Bernhard, T. J. Collins, *J. Am. Chem. Soc.* **2010**, *132*, 10990–10991.
- ⁷ J. Chen, J. W. Faller, R. H. Crabtree, G. W. Brudvig, *J. Am. Chem. Soc.* **2004**, *126*, 7345–7349.
- ⁸ (a) S. W. Gersten, G. J. Samuels, T. J. Meyer, *J. Am. Chem. Soc.* **1982**, *104*, 4029–4030; (b) J. A. Gilbert, D. S. Eggleston, W. R. Murphy, D. A. Geselowitz, S. W. Gersten, D. J. Hodgson, T. J. Meyer, *J. Am. Chem. Soc.* **1985**, *107*, 3855–3864; (c) C. Sens, I. Romero, M. Rodriguez, A. Llobet, T. Parella, J. Benet-Buchholz, *J. Am. Chem. Soc.* **2004**, *126*, 7798–7799; (d) R. Zong, R. P. Thummel, *J. Am. Chem. Soc.* **2005**, *127*, 12802–12803.
- ⁹ J. J. Concepcion, J. W. Jurss, J. L. Templeton, T. J. Meyer, *J. Am. Chem. Soc.* **2008**, *130*, 16462–16463.
- ¹⁰ G. Zhang, R. Zong, H. W. Tseng, R. P. Thummel, *Inorg. Chem.* **2008**, *47*, 990–998.
- ¹¹ (a) L. L. Duan, A. Fischer, Y. H. Xu, L. C. Sun, *J. Am. Chem. Soc.* **2009**, *131*, 10397–10399; (b) D. J. Wasylenko, C. Ganesamoorthy, B. D. Koivisto, M. A. Henderson, C. P. Berlinguette, *Inorg. Chem.* **2010**, *49*, 2202–2209; (c) M. Yoshida, S. Masaoka, K. Sakai, *Chem. Lett.* **2009**, *38*, 702–703.
- ¹² S. Romain, L. Vigara, A. Llobet, *Acc. Chem. Res.* **2009**, *42*, 1944–1953.
- ¹³ J. J. Concepcion, M. K. Tsai, J. T. Muckerman, T. J. Meyer, *J. Am. Chem. Soc.* **2010**, *132*, 1545–1557.
- ¹⁴ B. Meunier, S. P. De Viser, S. Shaik, *Chem. Rev.* **2004**, *104*, 3947–3980.
- ¹⁵ J. Nyhlén, L. L. Duan, B. Åkermark, L. C. Sun, T. Privalov, *Angew. Chem. Int. Ed.* **2010**, *49*, 1773–1777.
- ¹⁶ C. Sens, M. Rodriguez, I. Romero, A. Llobet, T. Parella, J. Benet-Buchholz, *Inorg. Chem.* **2003**, *42*, 8385–8394.
- ¹⁷ (a) F. Laurent, E. Plantalech, B. Donnadiou, A. Jimenez, F. Hernandez, M. Martinez-Ripoll, M. Biner, A. Llobet, *Polyhedron* **1999**, *18*, 3321–3331; (b) I. Romero, M. Rodriguez, A. Llobet, M. N. Collomb-Dunand-Sauthier, A. Deronzier, T. Parella, H. Sotekli-Evans, *J. Chem. Soc. Dalton Trans.* **2000**, 1689–1694; (c) X. Sala, I. Romero, M. Rodriguez, A. Llobet, G. Gonzalez, M. Martinez, J. Benet-Buchholz, *Inorg. Chem.* **2004**, *43*, 5403–5409; (d) X. Sala, E. Plantalech, A. Poater, M. Rodriguez, I. Romero, M. Sola, A. Llobet, S. Jansat, M. Gómez, H. Stoeckli-Evans, J. Benet-Buchholz, *Chem. Eur. J.* **2006**, *12*, 2798–2807.
- ¹⁸ (a) P. E. Anderson, G. B. Deacon, K. H. Haarmann, F. R. Keene, T. J. Meyer, D. A. Reitsma, B. W. Skelton, G. F. Strouse, N. C. Thomas, T. A. Treadway, T. A. White, *Inorg. Chem.* **1995**, *34*, 6145–6157; (b) K. R. Barqawi, A. Llobet, T. J. Meyer, *J. Am. Chem. Soc.* **1988**, *110*, 7751–7759.

-
- ¹⁹ M. Rodríguez, I. Romero, A. Llobet, A. Deronzier, M. Biner, T. Parella, H. Soteckli-Evans, *Inorg. Chem.* **2001**, *40*, 4150-4156.
- ²⁰ A. Llobet, P. Doppelt, T. J. Meyer, *Inorg. Chem.* **1988**, *27*, 514-520.
- ²¹ M.-H. V. Huynh, T. J. Meyer, *Chem. Rev.*, **2007**, *107*, 5004–5064.
- ²² Specfit is a trademark of Spectrum Software Associates.
- ²³ F. Bozoglian, S. Romain, M. Z. Ertem, T. K. Todorova, C. Sens, J. Mola, M. Rodríguez, I. Romero, J. Benet-Buchholz, X. Fontrodona, C. J. Cramer, L. Gagliardi, A. Llobet, *J. Am. Chem. Soc.* **2009**, *131*, 15176-15187.
- ²⁴ (a) Y. V. Geletii, B. Botar, P. Kögerler, D. A. Hillesheim, D. G. Musaev, C. L. Hill, *Angew. Chem. Int. Ed.* **2008**, *47*, 3896-3899; (b) A. Sartorel, M. Carraro, G. Scorrano, R. D. Zorzi, S. Geremia, N. D. McDaniel, S. Bernhard, M. Bonchio, *J. Am. Chem. Soc.* **2008**, *130*, 5006-5007; (c) A. Sartorel, A. Miro, E. Salvadori, S. Romain, M. Carraro, G. Scorrano, M. Di Valentin, A. Llobet, C. Bo, M. Bonchio, *J. Am. Chem. Soc.* **2009**, *131*, 1651-1653; (d) Y. Xu, T. Åkermark, V. Gyollai, D. Zou, L. Eriksson, L. Duan, R. Zhang, B. Åkermark, L. Sun, *Inorg. Chem.* **2009**, *48*, 2717-2719. (e) Y. Xu, A. Fischer, L. Duan, L. Tong, E. Gabrielsson, B. Åkermark, L. Sun, *Angew. Chem. Int. Ed.* **2010**, asap.
- ²⁵ (a) E. Masllorens, M. Rodríguez, I. Romero, A. Roglans, T. Parella, J. Benet-Buchholz, M. Poyatos and A. Llobet, *J. Am. Chem. Soc.* **2006**, *128*, 16, 5306-5307; (b) H.W. Tseng, R. Zong, J. T. Muckerman, R. Thummel, *Inorg. Chem.* **2008**, *47*, 11763-11773; (c) S. W. Kohl, L. Weiner, L. Schwartzburd, L. Konstantinovski, L. J. W. Shimon, Y. Ben-David, M. A. Iron and D. Milstein, *Science* **2009**, *324*, 74-77; (d) Z. Chen, J. J. Concepcion, J. F. Hull, P. G. Hoertz, T. J. Meyer, *Dalton Trans.* **2010**, *39*, 6950-6952; (e) D. J. Wasylenko, C. Ganesamoorthy, B. D. Koivisto, C. P. Berlinguette, *Eur. J. Inorg. Chem.* **2010**, 3135–3142.
- ²⁶ (a) J. England, Y. Guo, E. R. Farquhar, V. G. Young Jr., E. Münck, L. Que Jr. *J. Am. Chem. Soc.* **2010**, *132*, 8635-8644; (b) R. L. Shook, A. S. Borovik, *Inorg. Chem.* **2010**, *49*, 3646-3660.
- ²⁷ M. Rodríguez, I. Romero, C. Sens, A. Llobet, A. Deronzier, *Electrochim. Acta* **2003**, *48*, 1047-1054.
- ²⁸ “Sustainable Industrial Chemistry”. Eds. M. Ricci, D. Bianchi, R. Bortolo. Chapter 13. “Towards the Direct Oxidation of Benzene to Phenol”, F. Cavani, G. Centi, S. Perathoner, F. Trifiro. **2009** Wiley-VCH Verlag GmbH & Co. KgaA.
- ²⁹ (a) Y. V. Geletii, Z. Huang, Y. Hou, D. G. Musaev, T. Lian, C. L. Hill, *J. Am. Chem. Soc.* **2009**, *131*, 7522-7523; (b) M. Orlandi, R. Argazzi, A. Sartorel, M. Carraro, G. Scorrano, M. Bonchio, F. Scandola, *Chem. Commun.* **2010**, *46*, 4725-4727; (c) F. Puntoriero, G. L. Ganga, A. Sartorel, M. Carraro, G. Scorrano, M. Bonchio, S. Campagna, *Chem. Commun.* **2010**, *46*, 4725-4727; (d) Y. Xu, L. Duan, L. Tong, B. Åkermark, L. Sun, *Chem. Commun.* **2010**, *46*, 6506-6508.
- ³⁰ E. Dulière, M. Devillers, J. Marchand-Brynaert, *Organometallics* **2003**, *22*, 804-811.
- ³¹ W. S. Yu, C. C. Cheng, Y. M. Cheng, P. C. Wu, Y. H. Song, Y. Chi, P. T. Chou, *J. Am. Chem. Soc.* **2003**, *125*, 10800-10801.

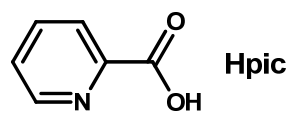
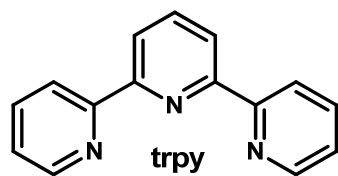
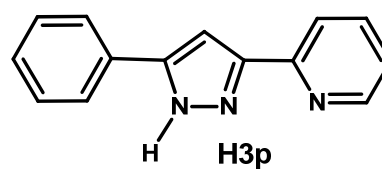
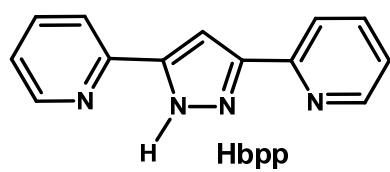
³² Data collection with APEX II v2009.1-02. Bruker (2007). Bruker AXS Inc., Madison, Wisconsin, USA.

³³ Data reduction with Bruker SAINT V7.60A. Bruker (2007). Bruker AXS Inc., Madison, Wisconsin, USA.

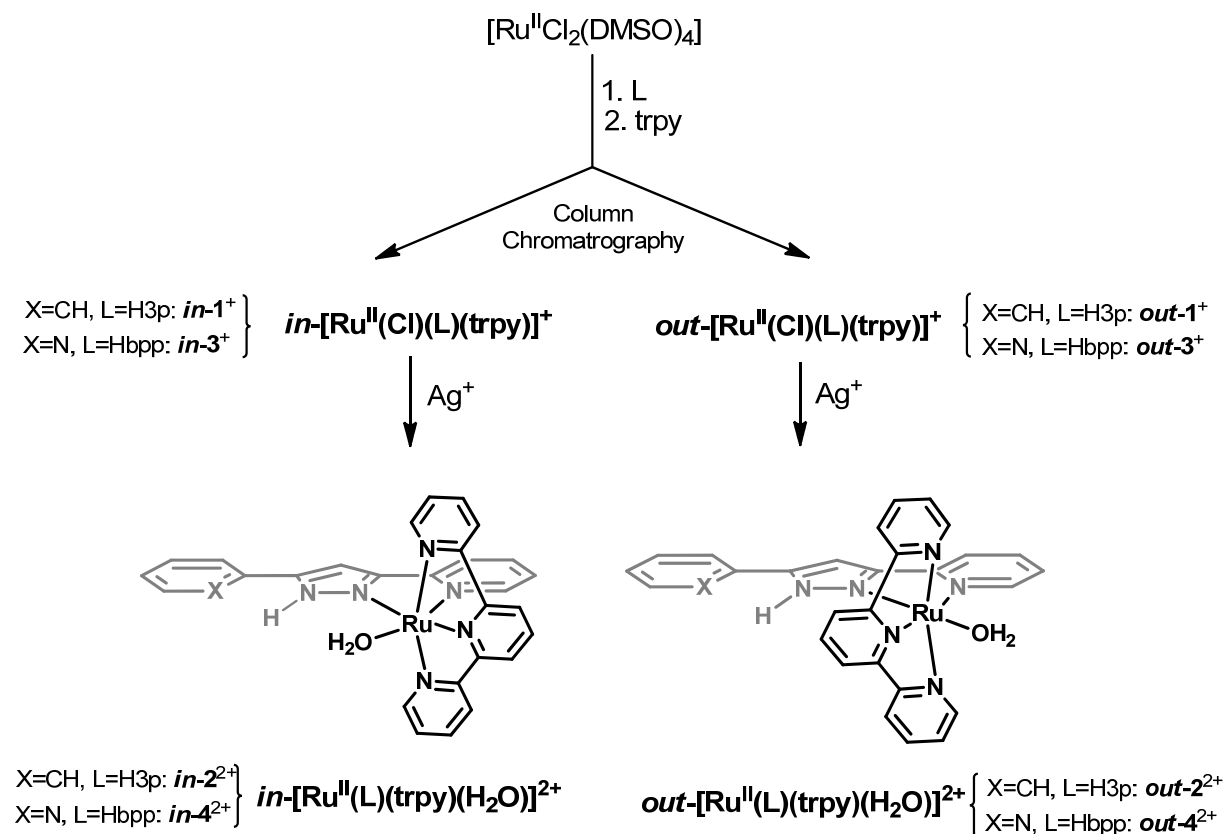
³⁴ SADABS: V2008/1 Bruker (2001). Bruker AXS Inc., Madison, Wisconsin, USA. Blessing, *Acta Cryst.* (1995) A51 33-38.

³⁵ Sheldrick, G.M. *Acta Cryst.* **2008** A64, 112-122. SHELXTL V6.14.

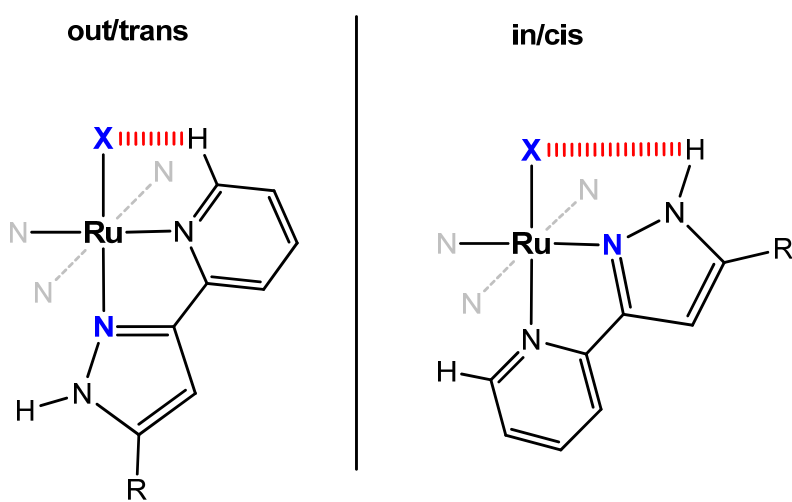
Chart 1. The ligands



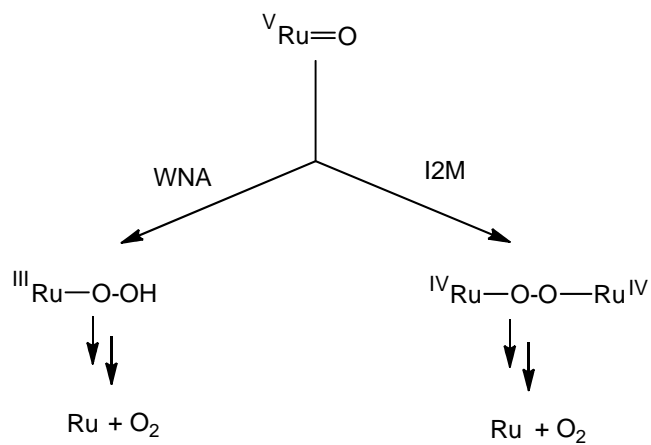
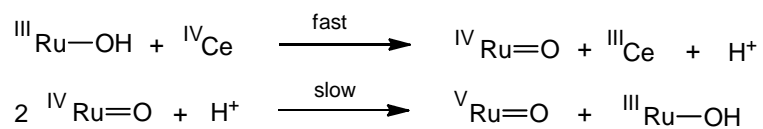
Scheme 1. Synthetic strategy and numbering scheme.



Scheme 2. Schematic drawing of the *in*- and *out*-[Ru(X)(trpy)(L)]^{h+} complexes indicating the X---H interaction (X = Cl or H₂O; L = Hbpp, R = 2-pyridyl; L = H3p R = phenyl). The N coordinating atoms of the trpy ligand are shown in grey and the rest of the ligand is not shown for clarity purposes. The equivalency between the *in*/*cis* and *out*/*trans* isomers is also indicated. See text for further details.



Scheme 3. Potential O-O bond formation pathways following the generation of high oxidation states.



Scheme 4. Sequence of reaction that illustrate the photochemically induced catalytic water oxidation

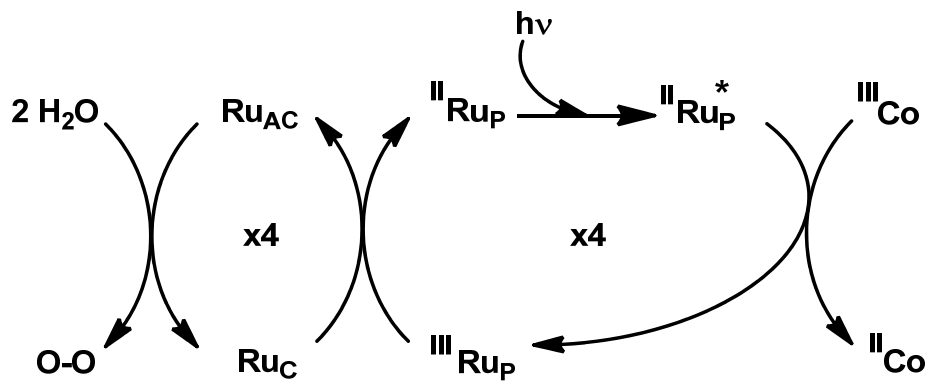


Table 1. X-ray diffraction parameters.

Compound	<i>out-1</i> (PF ₆)	<i>in-1</i> (PF ₆)
Empirical formula	C ₃₂ H ₃₀ ClF ₆ N ₆ O ₂ PRu	C _{32.25} H ₂₉ ClF ₆ N ₆ OPRu
Formula weight	812.11	798.10
Temperature	100(2) K	100(2) K
Wavelength	0.71073 Å	0.71073 Å
Crystal system	Triclinic	Triclinic
Space group	P-1	P-1
Unit cell dimensions	a = 8.8548(14) Å α = 71.790(4) ° b = 13.0005(15) Å β = 83.378(6) ° c = 16.799(2) Å γ = 79.578(6) °	a = 11.6693(5) Å α = 72.287(2) ° b = 12.1900(5) Å β = 89.621(2) ° c = 12.2548(6) Å γ = 84.141(2) °
Volume	1803.1(4) Å ³	1651.36(13) Å ³
Z	2	2
Density (calculated)	1.496 Mg/m ³	1.605 Mg/m ³
Absorption coefficient	0.622 mm ⁻¹	0.675 mm ⁻¹
F(000)	820	805
Crystal size	0.06 x 0.02 x 0.02 mm ³	0.30 x 0.01 x 0.01 mm ³
Theta range for data collection	1.77 to 36.47 °	1.75 to 36.42 °
Index ranges	-19 ≤ h ≤ 19, -21 ≤ k ≤ 21, -20 ≤ l ≤ 19	-19 ≤ h ≤ 19, -20 ≤ k ≤ 20, -20 ≤ l ≤ 19
Reflections collected	15485	14550
Independent reflections	12771 [R(int) = 0.0595]	11827 [R(int) = 0.0513]
Completeness to theta	=36.47 °, 0.875 %	=36.42 °, 0.901 %
Absorption correction	Empirical	Empirical
Max. and min. transmission	1.00 and 0.82	0.9933 and 0.8231
Refinement method	Full-matrix least-squares on F ²	Full-matrix least-squares on F ²
Data / restraints / parameters	15485 / 78 / 581	14550 / 138 / 543

Goodness-of-fit on F2	1.197	1.028
Final R indices [I>2sigma(I)]	R1 = 0.0745 wR2 = 0.2150	R1 = 0.0457 , wR2 = 0.1115
R indices (all data)	R1 = 0.0908 wR2 = 0.2237	R1 = 0.0605 , wR2 = 0.1208

Table 2. Electrochemical and absorption spectral data for complexes **1-6**.

Complex	E^0 (V) ^a	λ_{\max} (ϵ)	assignment	entry	
<i>Ru-Cl</i>	<i>in-1</i> ⁺	0.81	240 (40200), 276 (33200), 282 (33200), 318 (33400) 419 (6300), 487 (7200), 594 (1500), 657 (800)	π - π^* $d\pi$ - π^* d-d	1
	<i>out-1</i> ⁺	0.69	241 (47000), 277 (37700), 282 (37800), 323 (34400) 413 (7100), 502 (8200) 600 (1500), 657 (1400)	π - π^* $d\pi$ - π^* d-d	2
	<i>in-3</i> ⁺	0.86	239 (42000), 277 (35800), 319 (37500) 354 (13500), 419 (7400), 494 (8000) 600 (1800), 665 (1000)	π - π^* $d\pi$ - π^* d-d	3
	<i>out-3</i> ⁺	0.63	241 (41700), 282 (35200), 323 (31000) 377 (9800), 415 (7100), 505 (7800) 600 (1400), 660 (1300)	π - π^* $d\pi$ - π^* d-d	4
	<i>cis-5</i> ^b	0.46			5
	<i>trans-5</i> ^b	0.39			6
<i>Ru-OH₂</i>	<i>in-2</i> ²⁺	0.785, --, --	273 (34300), 279 (34700), 314 (33700) 392 (5200), 460 (7100)	π - π^* $d\pi$ - π^*	7
	<i>out-2</i> ²⁺	0.67, 1.00, 1.46	273 (39000), 279 (39600), 316 (35200) 390 (6600), 475 (7400)	π - π^* $d\pi$ - π^*	8
	<i>in-4</i> ²⁺	0.66, --, 1.46	313 (25500) 394 (8700), 458 (9300)	π - π^* $d\pi$ - π^*	9
	<i>out-4</i> ²⁺	0.62, 1.07, 1.46	278 (39400), 313 (33800) 404 (9600), 458 (10700)	π - π^* $d\pi$ - π^*	10
	<i>cis-6</i> ^{+,b}	0.58, 1.12, --			11
	<i>trans-6</i> ^{+,b}	0.50, 0.90, --			12

^a For the Ru-Cl complexes the potential refers to the Ru(III)/Ru(II) couple. For the Ru-OH₂ complexes it refers to the three successive redox waves obtained that are attributed to the following couples in this order: Ru(III)/Ru(II), Ru(IV)/Ru(III) and Ru(V)/Ru(IV). See text for further details.

^b See reference 20.

Figure 1. Ortep ellipsoid (50 % probability) for the molecular structure of the cationic part of: left, *out-1*⁺; and right, *in-1*⁺. Color codes: Ru, cyan; Cl, green; N, blue; C, gray; H, light blue.

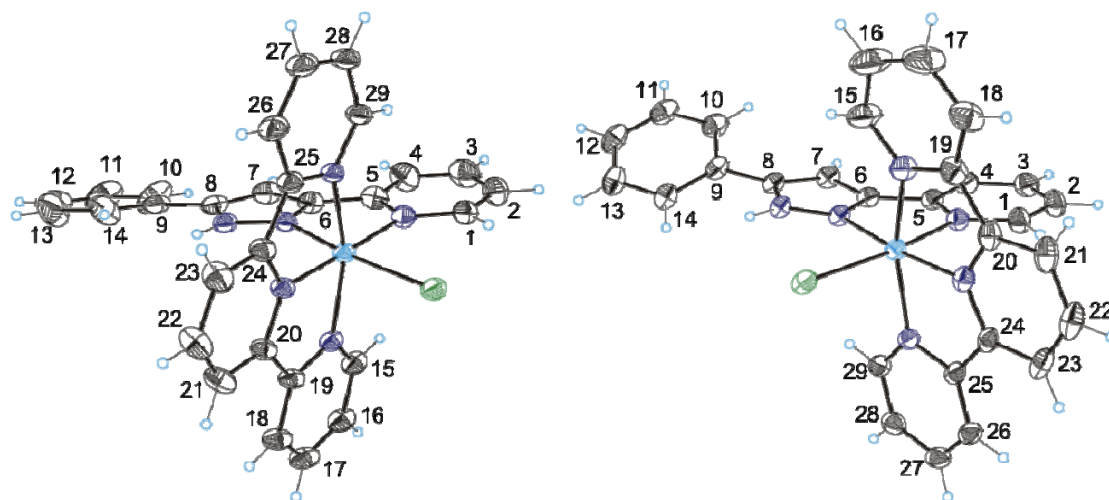


Figure 2. ^1H -NMR of *out-1*⁺ (top) and *in-1*⁺ (bottom) in d_6 -DMSO. The resonance of the H1 proton is indicated in each spectrum. The rest of protons are assigned in the experimental section.

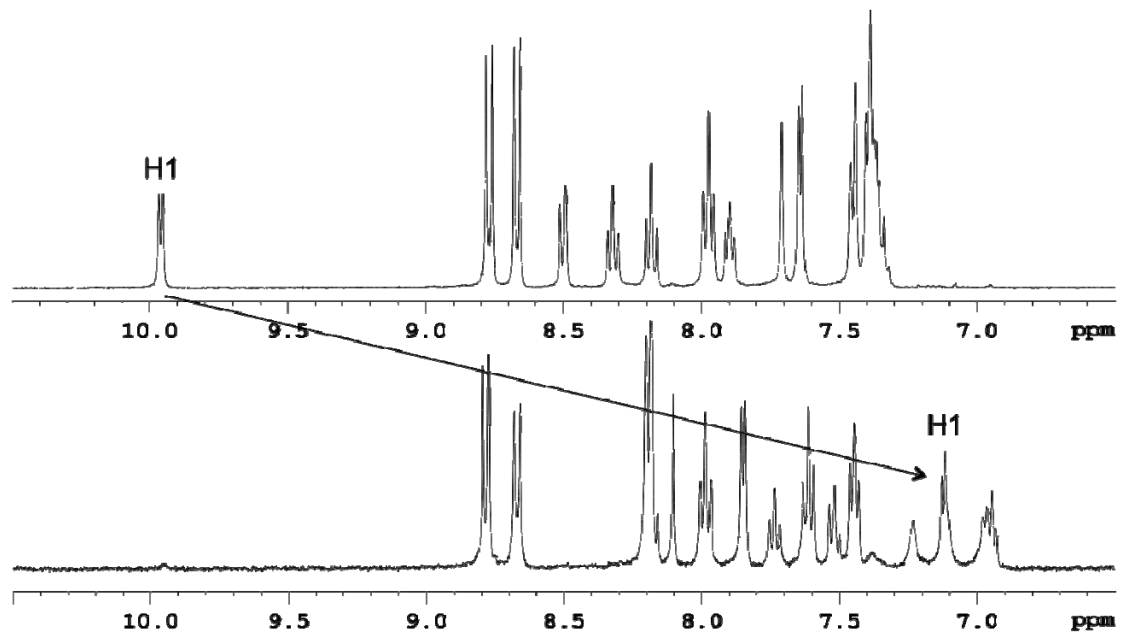


Figure 3. UV-Vis spectra of *out-1*⁺ in DCM (solid) and *out-2*²⁺ in CF₃SO₃H (pH = 1.0) (dashed).

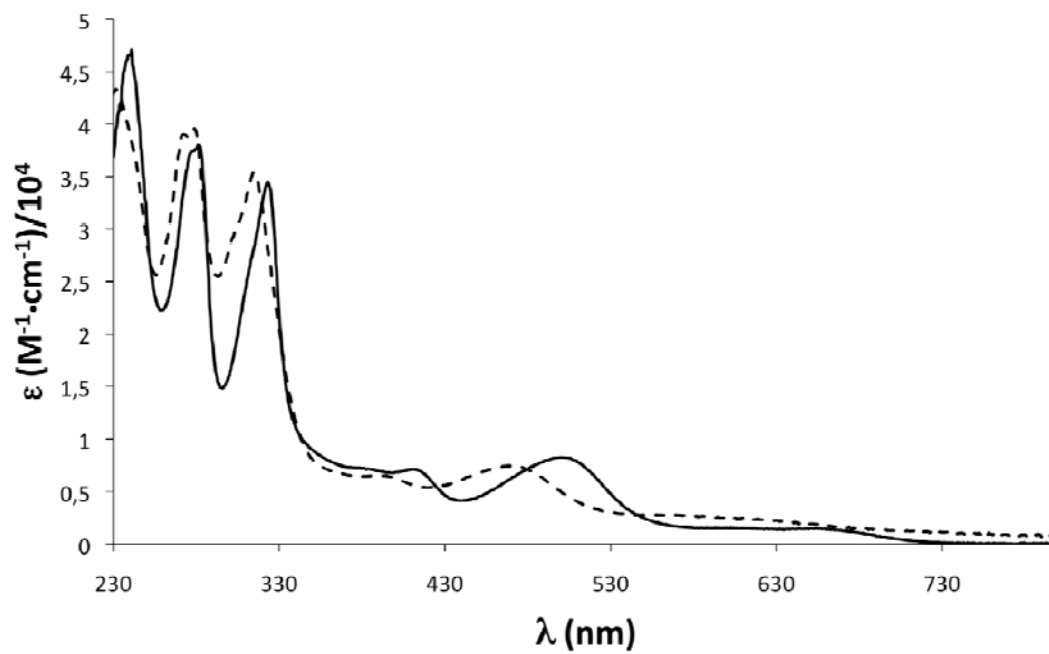


Figure 4. Redox properties of complex $out-2^{2+}$ in 0.1M triflic acid using a glassy carbon disk electrode, Pt wire as auxiliary and SSCE as reference electrode. Solid line and dashed line are CVs performed at 50 mV/s for $out-2^{2+}$. The dot-dashed line is the background CV in the absence of complex $out-2^{2+}$. Dotted line is a SWV of $out-2^{2+}$ (Step E = 4 mV, SW Amplitude = 25 mV, SW Frequency = 15 Hz).

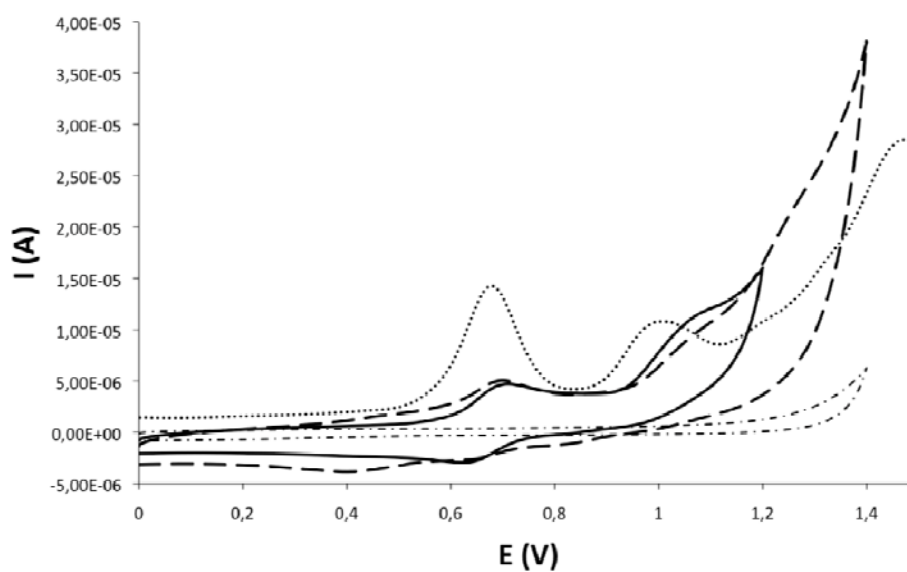


Figure 5. UV-vis spectral changes obtained upon addition of 1 equivalent of Ce(IV) to *out-4*³⁺ (Ru(III)) 0.1 mM (data recorded every 30 s, for clarity only every 3rd spectra is presented). Arrow indicates the principle absorption change. Inset, absorption vs. time plot at $\lambda = 544$ nm (empty diamonds) and mathematical simulation (red solid line) assuming WNA mechanism. See text for details.

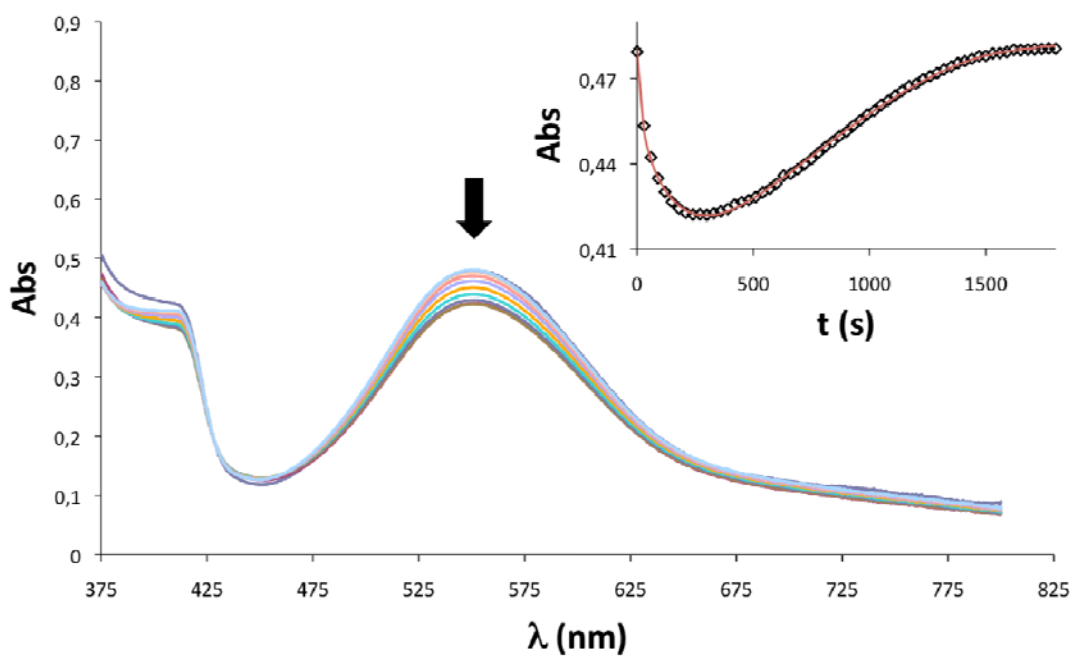


Figure 6. Oxygen evolution profile (black line) in solution obtained upon addition of 1 equivalent of Ce(IV) to *out-4*³⁺ (Ru(III)) 0.2 mM in 0.1M triflic acid solution and mathematical simulations assuming the I2M (blue line) and WNA (red line) mechanisms.

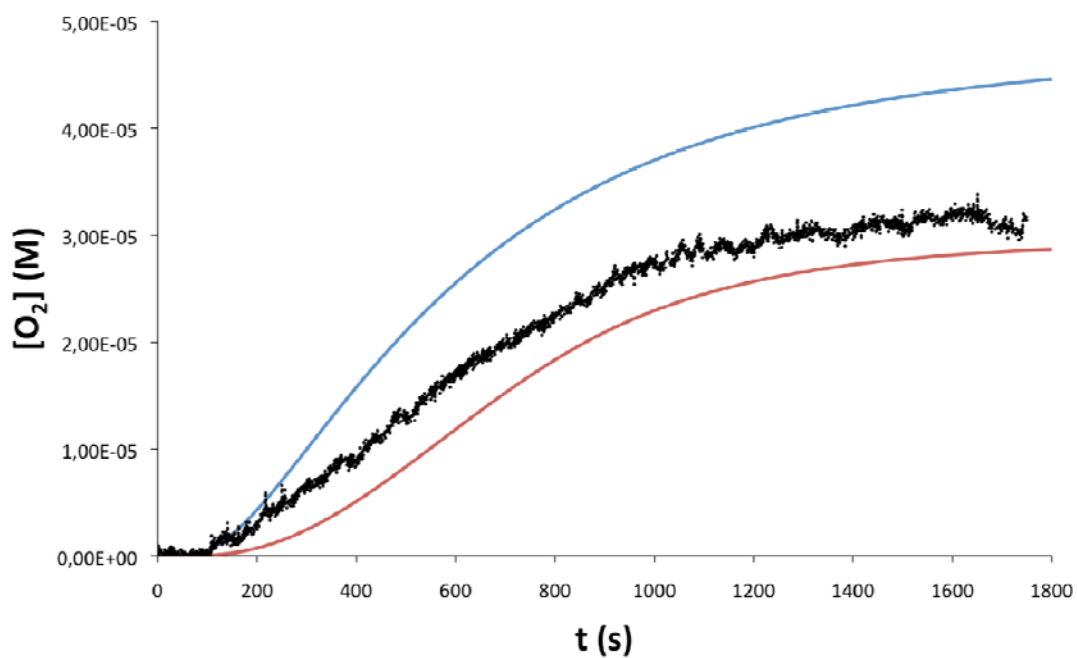


Figure 7. Gas evolution profile monitored manometrically upon treatment of 1.0 mM WOCs *out-2*²⁺ (dashed dotted), *in-2*²⁺ (dotted), *out-4*²⁺ (solid) and *in-4*²⁺ (dashed) with 100 mM Ce(IV) in a 0.1 M CF₃SO₃H solution.

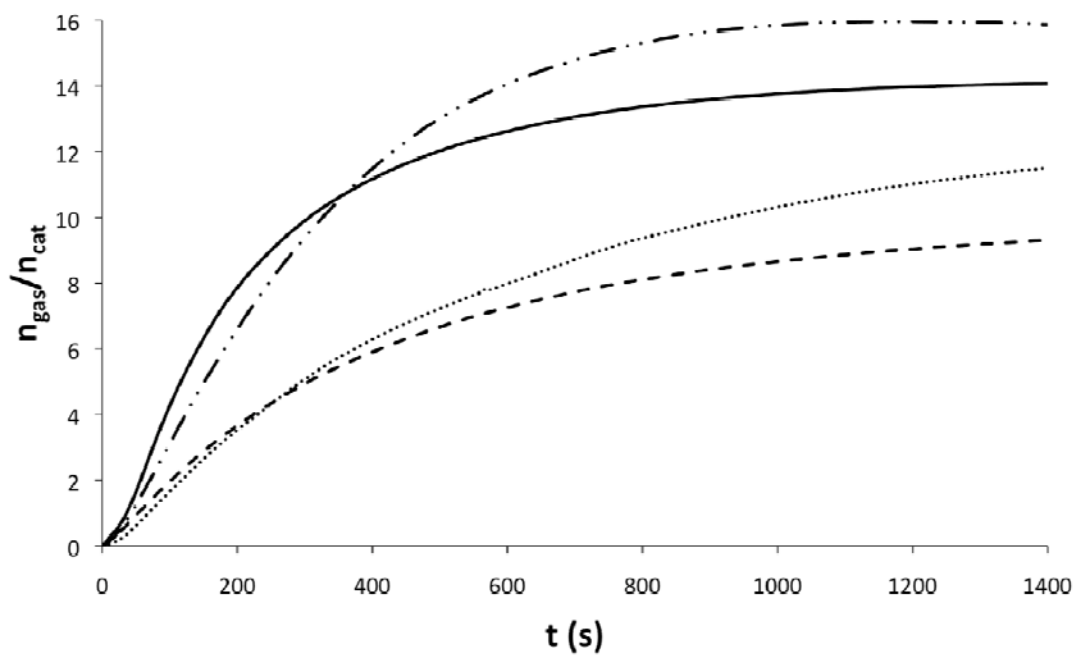
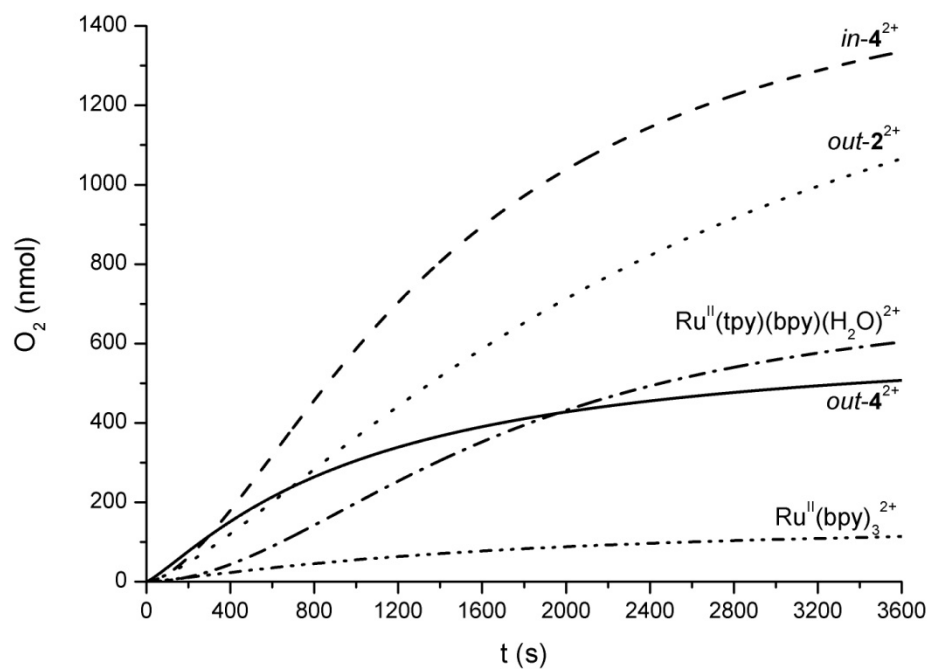
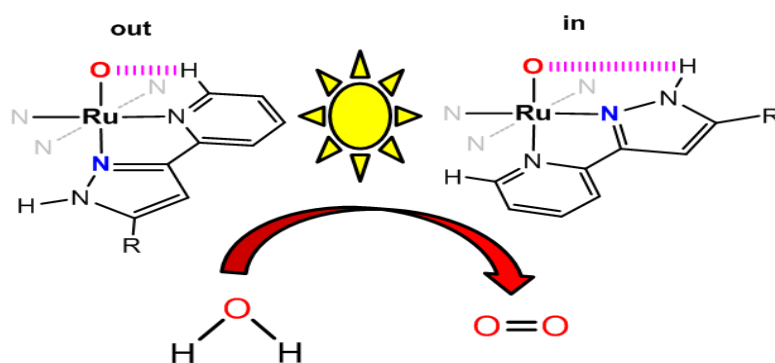


Figure 8. Oxygen evolution profile photochemically induced by complexes 2^{2+} , 4^{2+} and $[\text{Ru}(\text{trpy})(\text{bpy})(\text{H}_2\text{O})]^{2+}$ at pH = 7.0 in a phosphate solution at 20.0 °C, upon irradiation with a 300 W Xenon lamp with a 400 nm filter. $[\text{Co}^{\text{III}}(\text{Cl})(\text{NH}_3)_5]^{2+}$ was used as a sacrificial electron acceptor and $[\text{Ru}(\text{bpy})_3]^{2+}$ as photosensitizer.



TOC GRAPHIC

A family of new mononuclear Ru-aqua complexes is reported that are capable of acting as water oxidation catalysts chemically, electrochemically and photochemically. Their performance is rationalized based on electronic and geometric factors



SUPPORTING INFORMATION FOR:

Chemical, Electrochemical and Photochemical Catalytic Oxidation of Water to Dioxygen with Mononuclear Ru Complexes

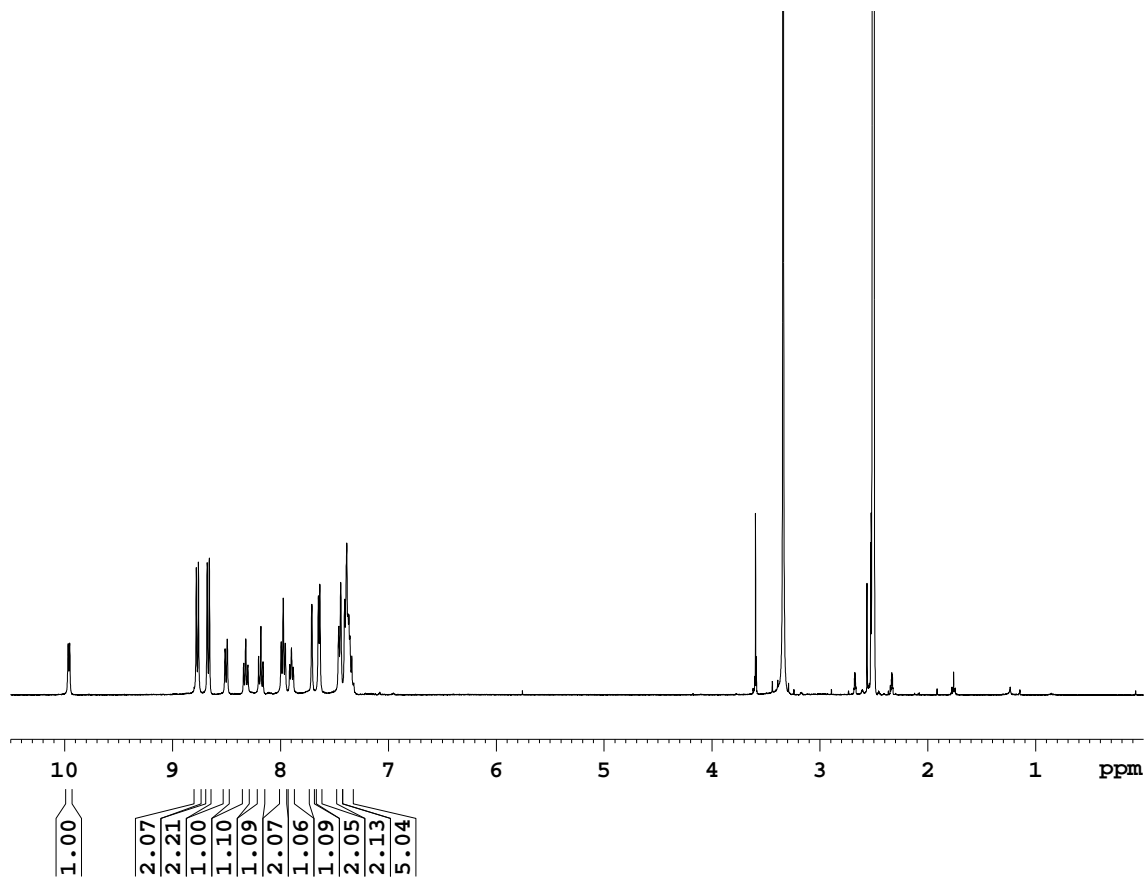
Stephan Roeser,^a Pau Farràs,^a Fernando Bozoglian,^a Marta Martínez,^a Jordi Benet-Buchholz^a and Antoni Llobet^{a,b,*}

^aInstitute of Chemical Research of Catalonia (ICIQ), Av. Països Catalans 16, E-43007 Tarragona, Spain and ^bDepartament de Química, Universitat Autònoma de Barcelona, Cerdanyola del Vallès, E-08193 Barcelona, Spain.

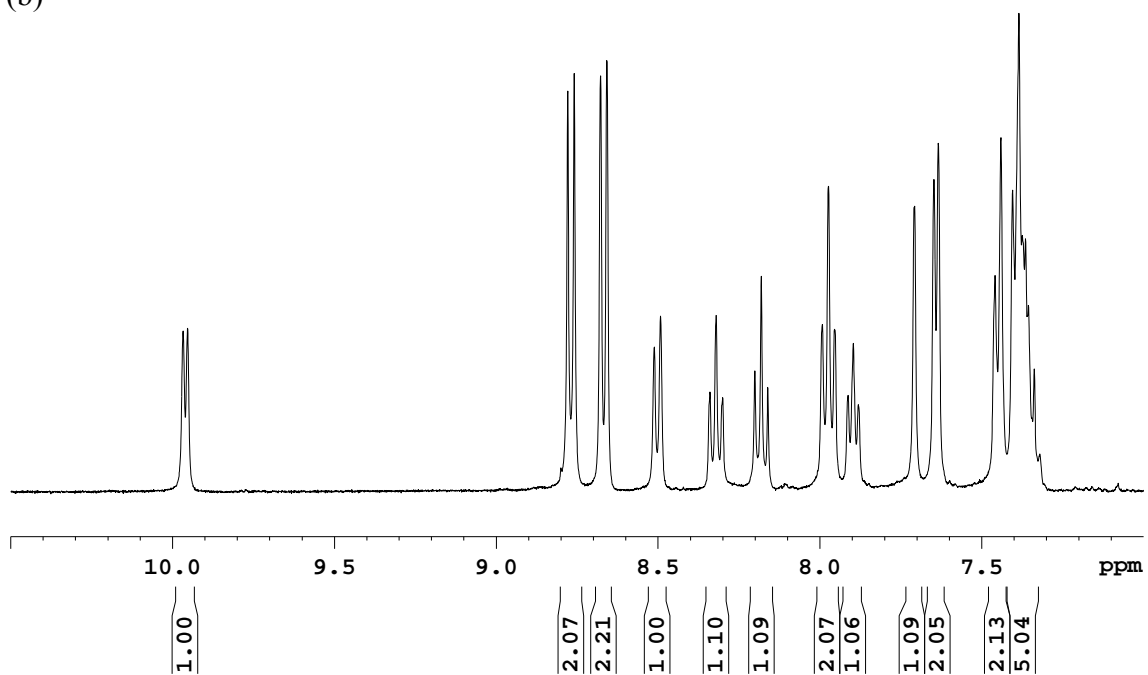
email: allobet@iciq.es

Figure S1. 1D and 2D NMR spectra (400 MHz, 298 K, d₆-DMSO for complex *out-1*⁺: (a) ¹H-NMR, (b) aromatic region of ¹H-NMR, (c) ¹³C{¹H}-NMR, (d) COSY-NMR (e) HMQC-NMR and (f) HMBC-NMR.

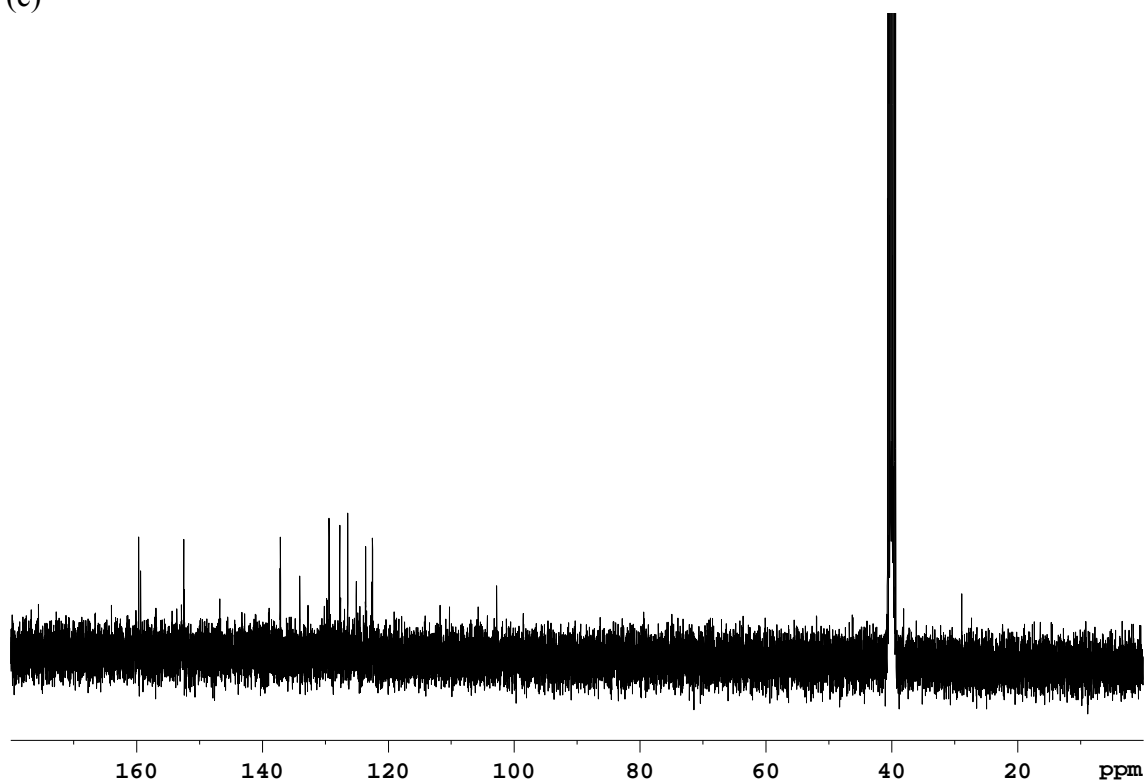
(a)



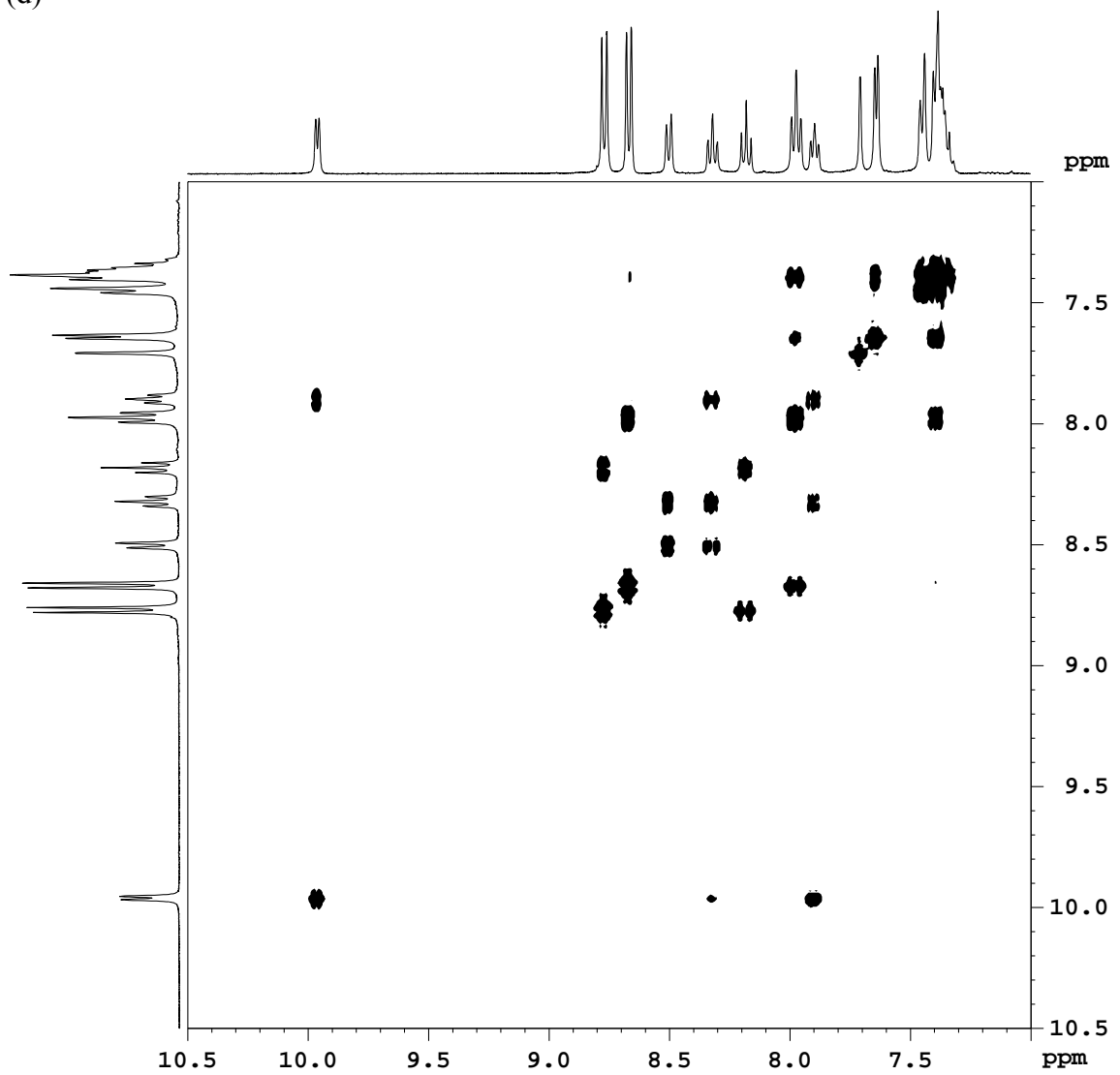
(b)



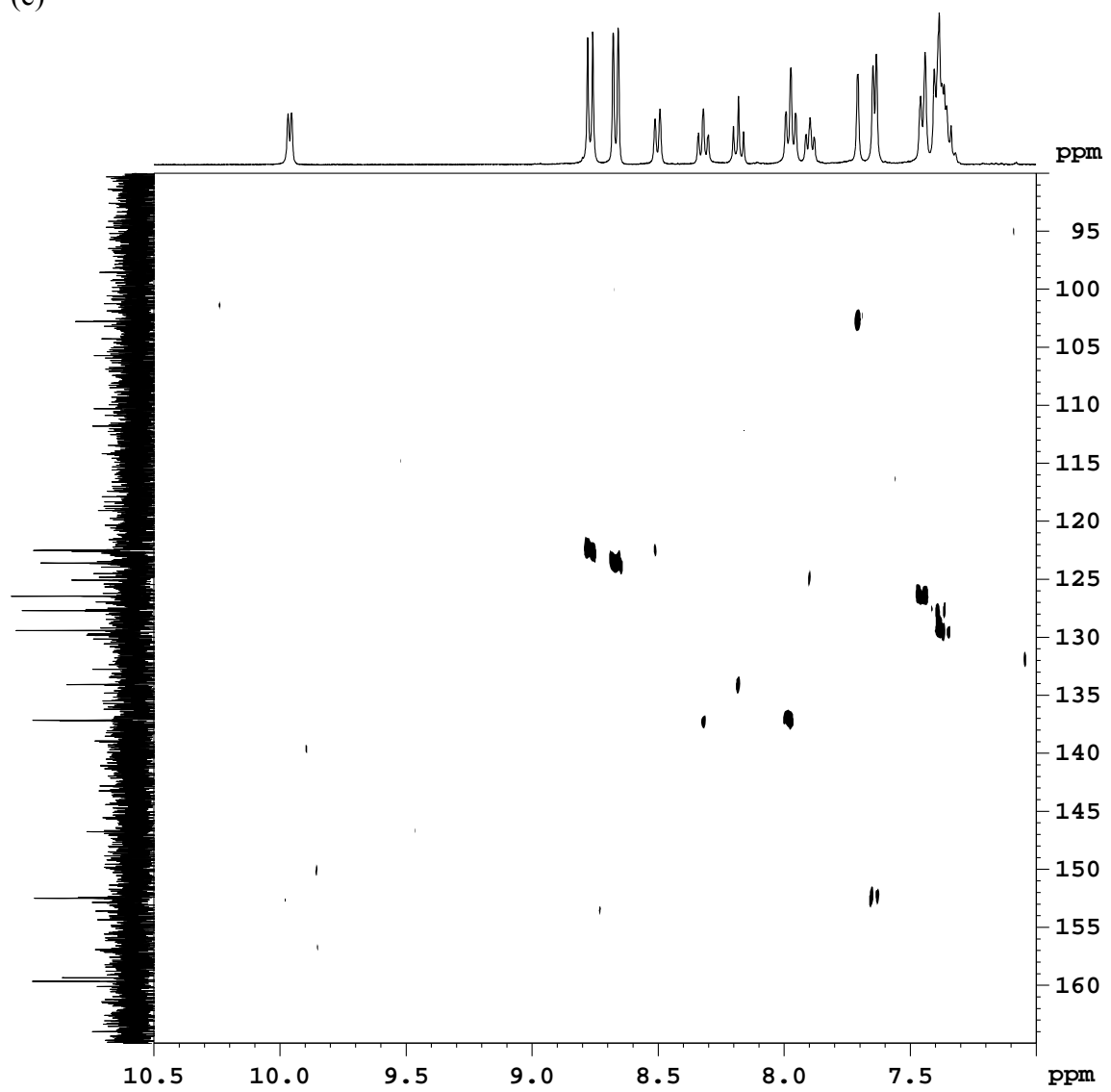
(c)



(d)



(e)



(f)

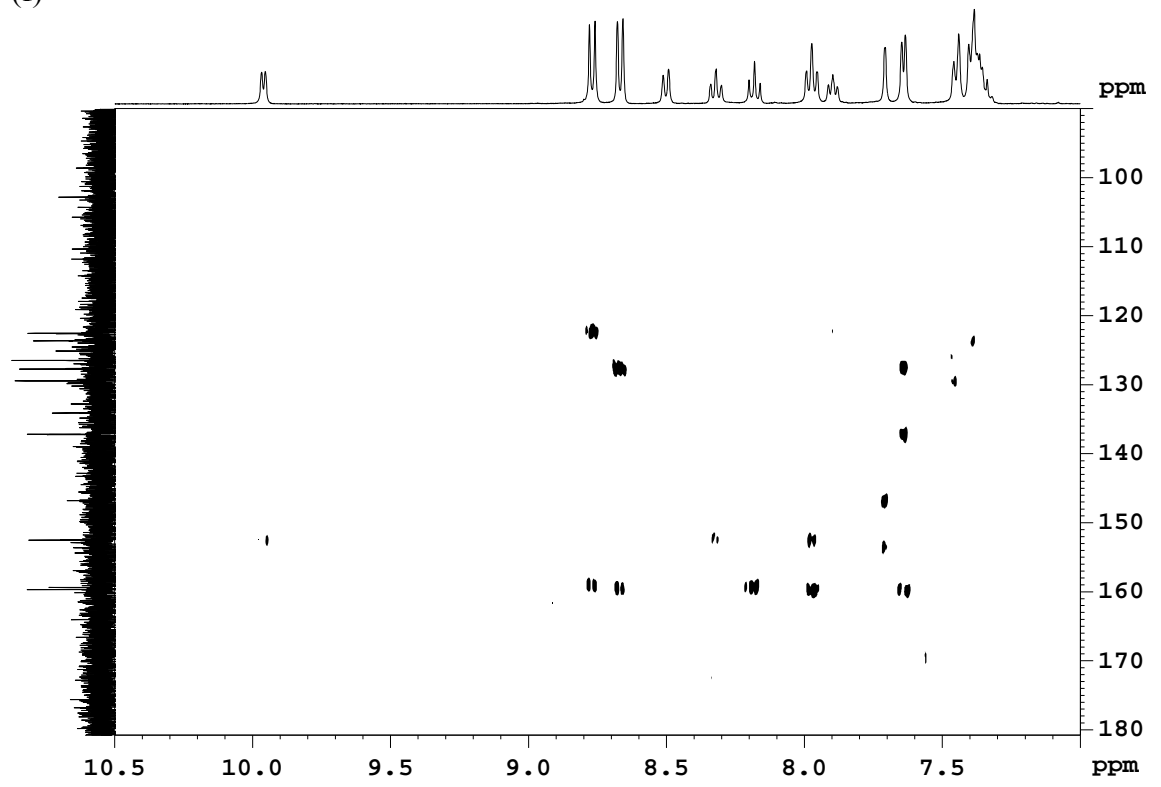
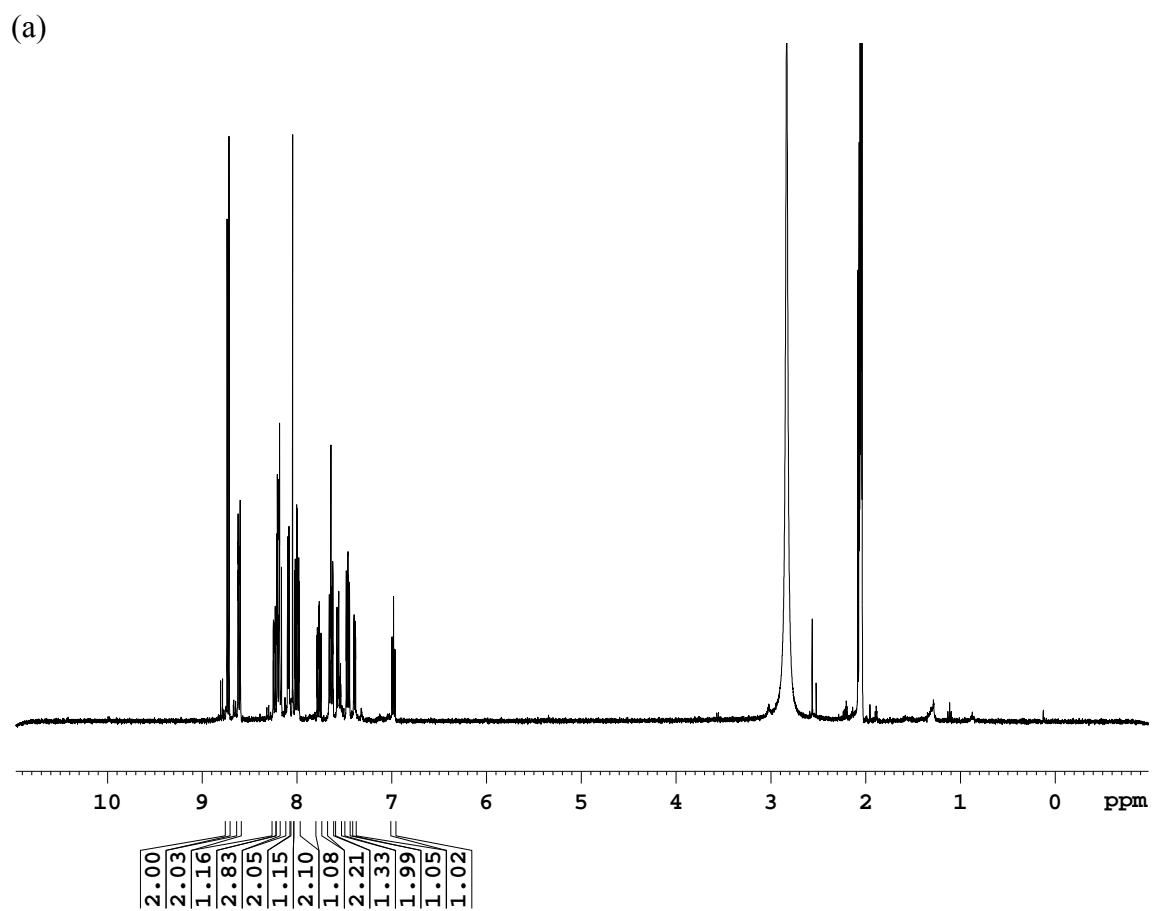
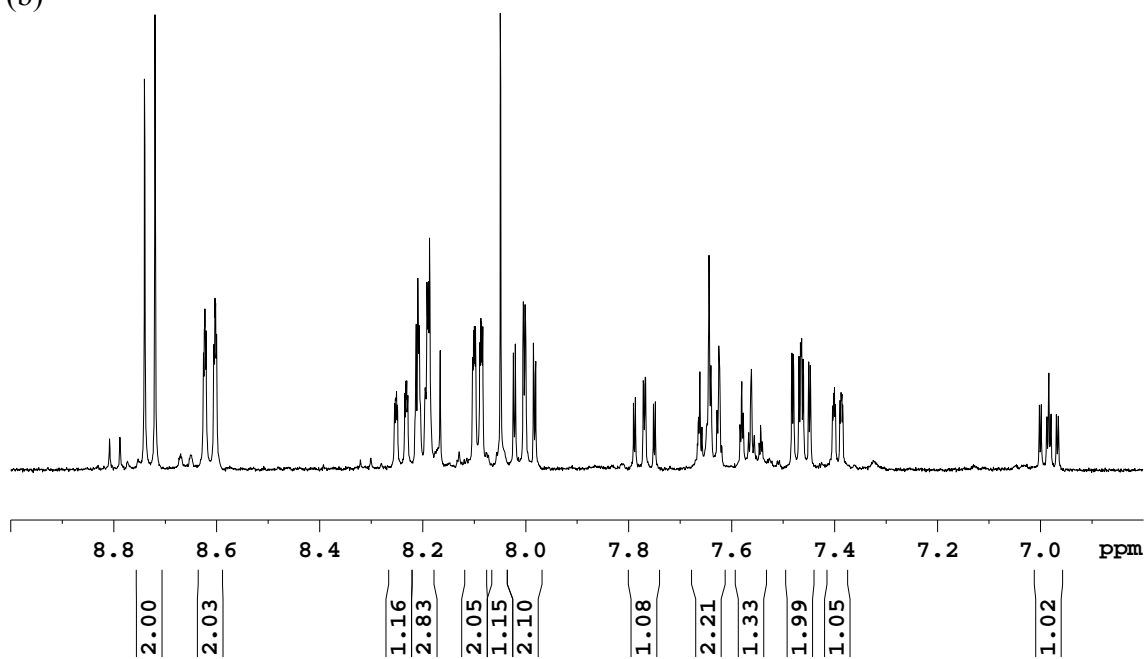


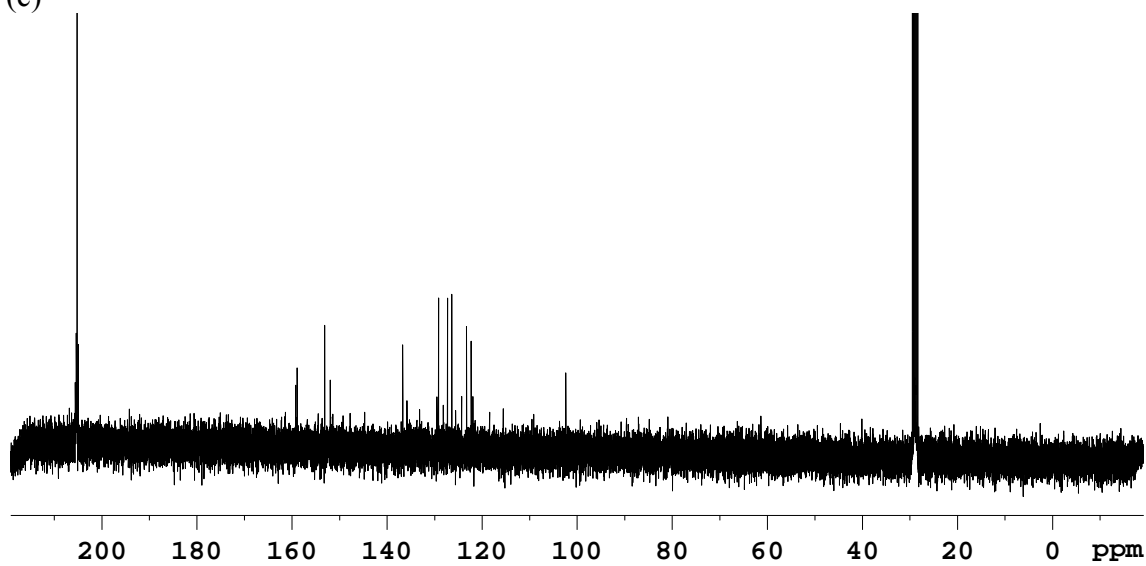
Figure S2. 1D and 2D NMR spectra (400 MHz, 298 K, d₆-DMSO for complex *in-1*⁺: (a) ¹H-NMR, (b) aromatic region of ¹H-NMR, (c) ¹³C{¹H}-NMR, (d) COSY-NMR (e) HMQC-NMR and (f) HMBC-NMR.



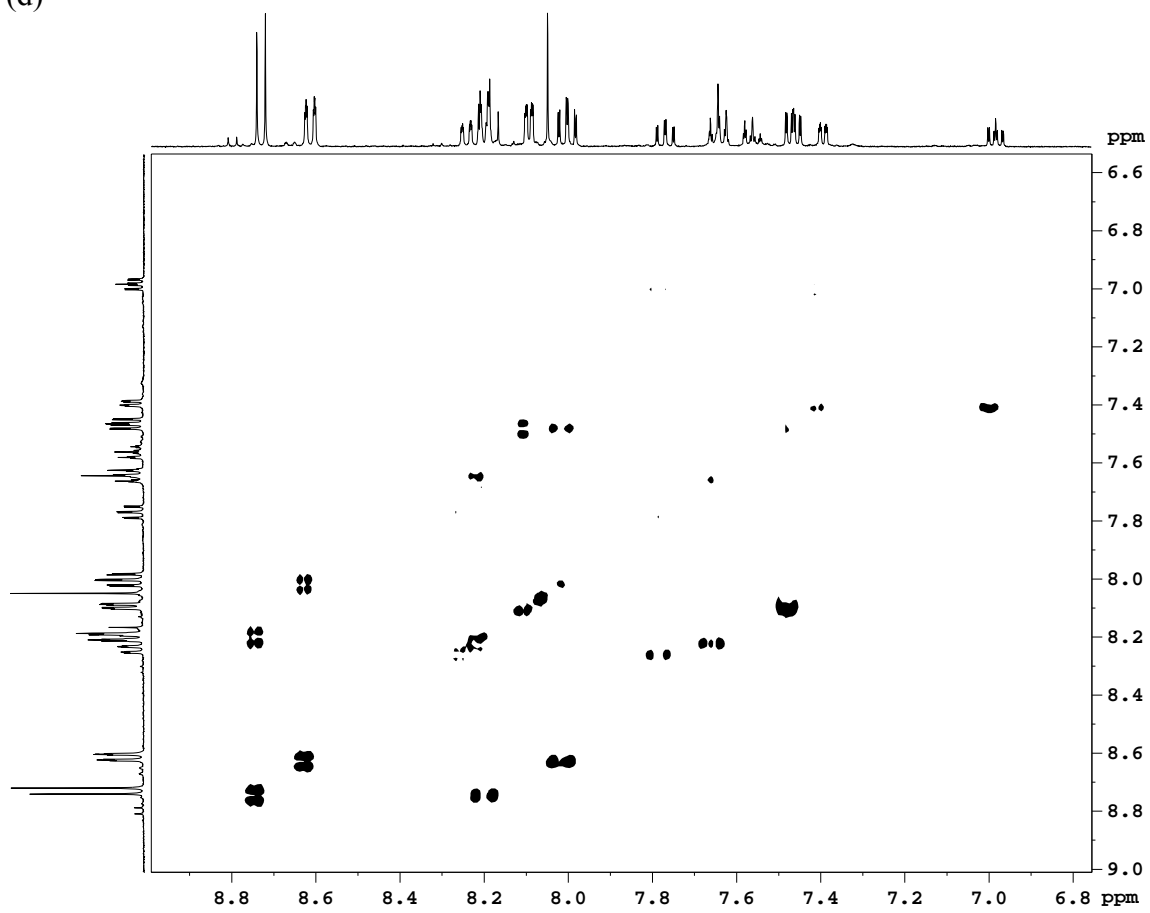
(b)



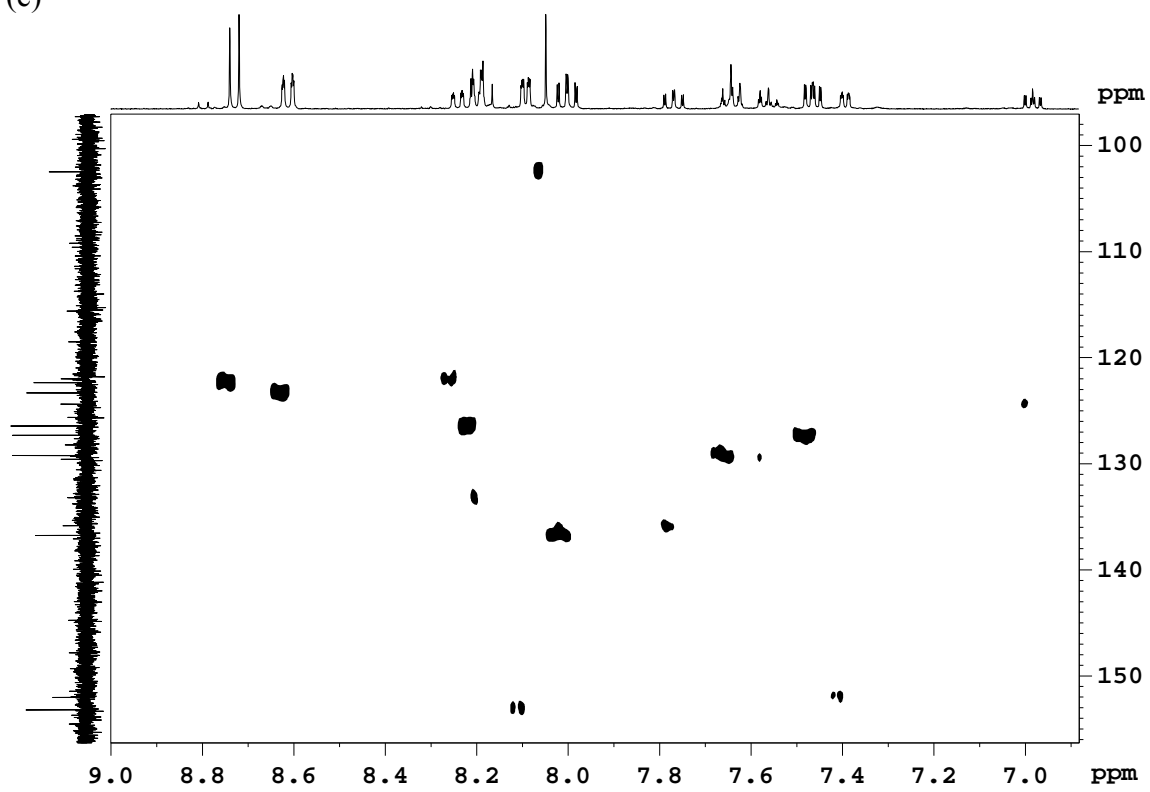
(c)



(d)



(e)



(f)

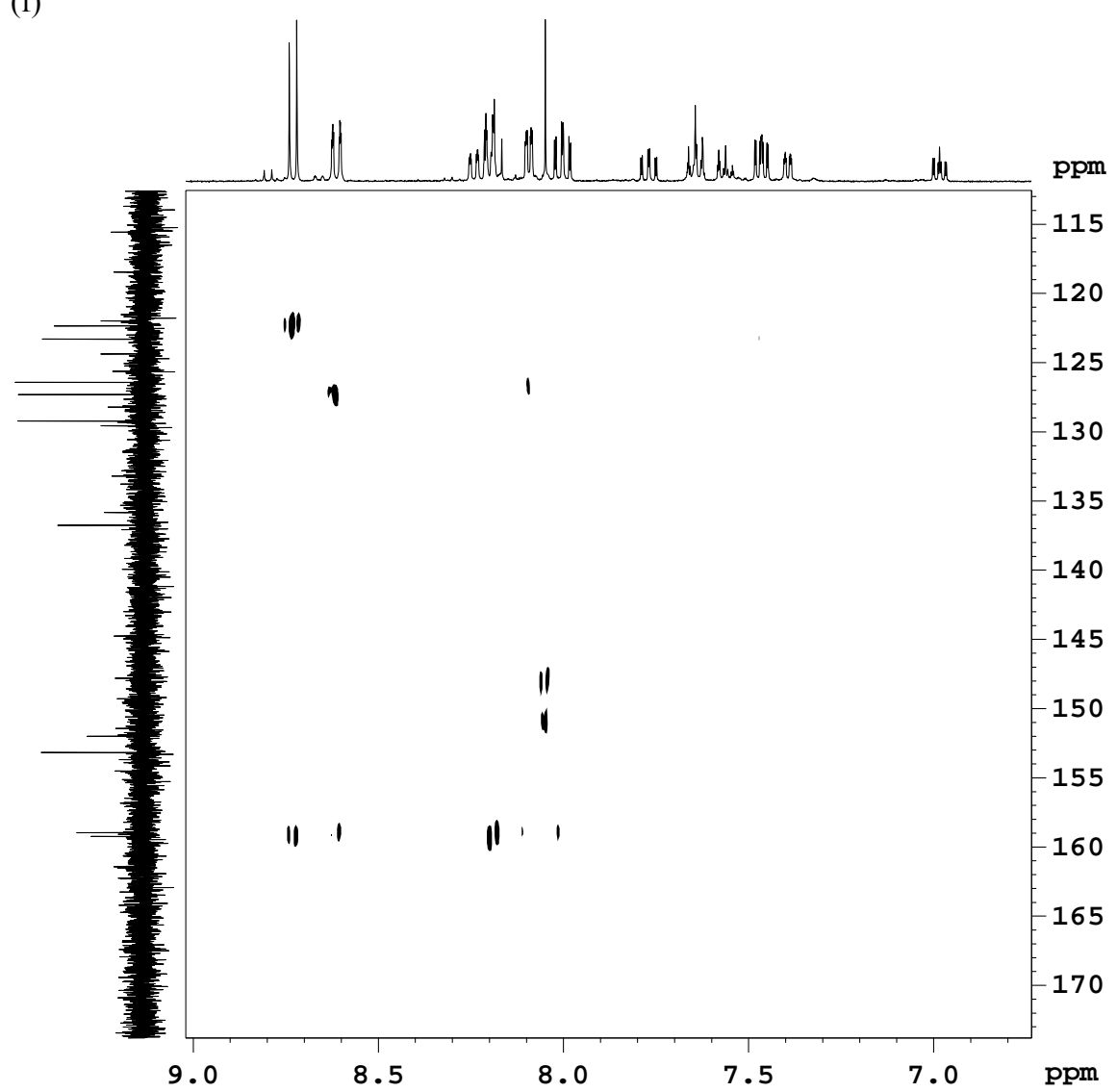


Figure S3. UV-Vis spectra of *out-1*⁺ (dotted-dashed), *in-1*⁺ (dotted), *out-3*⁺ (solid) and *in-3*⁺ (dashed) in DCM.

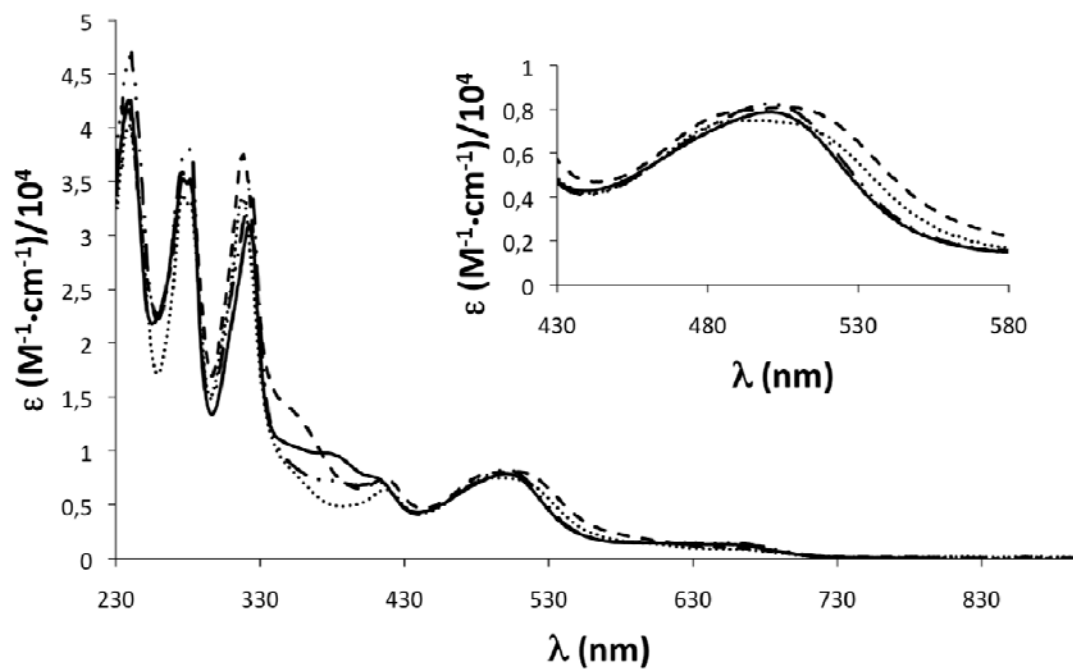


Figure S4. UV-Vis spectra of *out-2*²⁺ (dotted-dashed), *out-4*²⁺ (solid) and *in-4*²⁺ (dashed) in CF₃SO₃H (pH = 1.0).

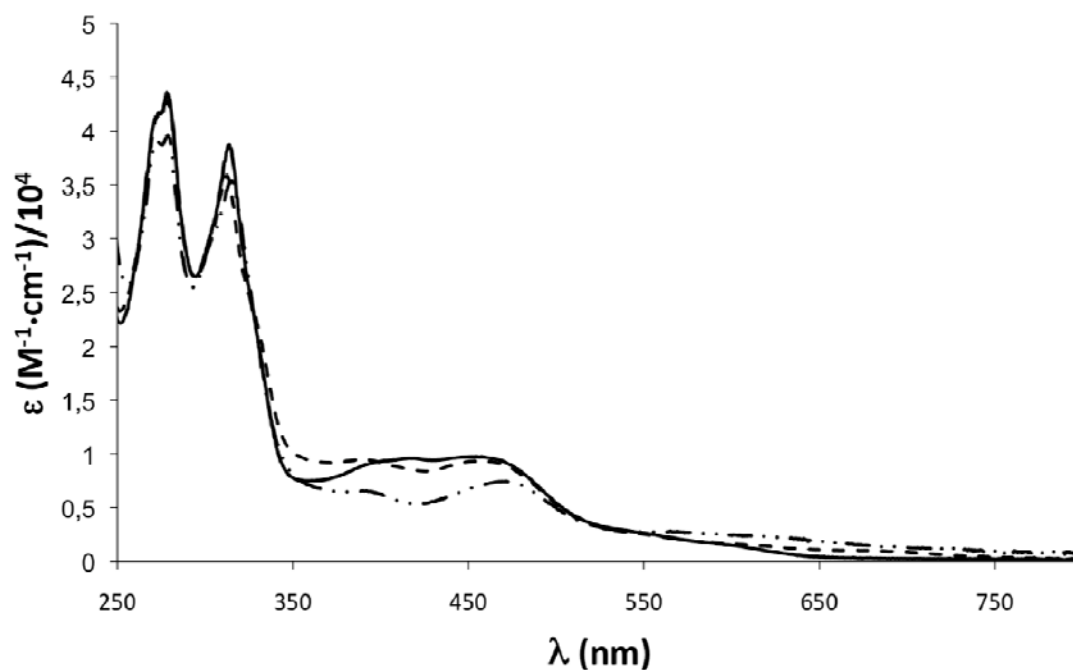


Figure S5. Uv-Vis redox titration; addition of 13 x 2 μL of oxidant solution to a 3 mL sample of *out-2*²⁺ ($[\text{Ru}] = 1.56 \cdot 10^{-5} \text{ M}$), oxidant = Ce(IV) ($[\text{Ce(IV)}] = 1.81 \text{ mM}$) in $\text{CF}_3\text{SO}_3\text{H}$ (pH = 1.0). Inset shows the change in absorption at 312 nm (green + orange triangles).

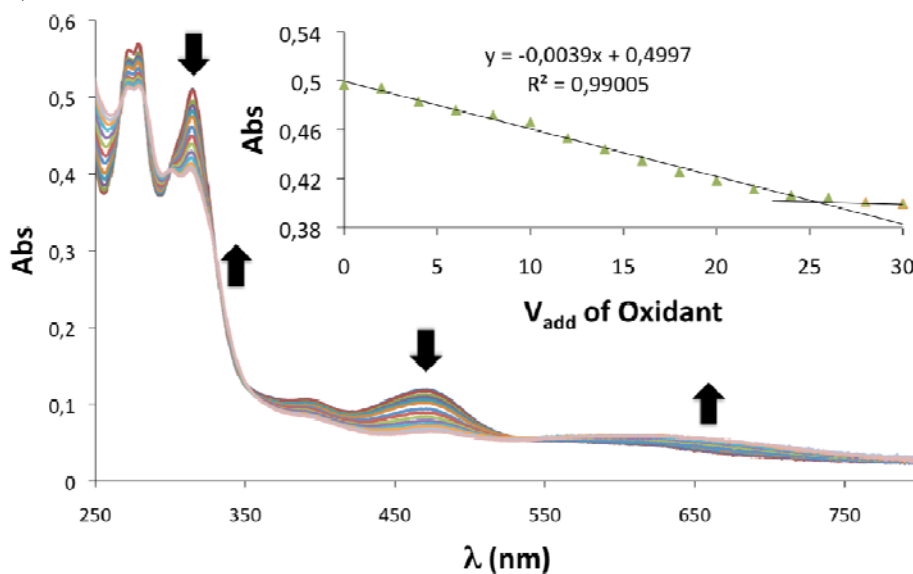


Figure S6. Uv-Vis redox titration; addition of 5 x 4 μL of oxidant to a 3 mL sample solution of *out-4*²⁺ ($[\text{Ru}] = 4.25 \cdot 10^{-5} \text{ M}$), oxidant = Ce(IV) ($[\text{Ce(IV)}] = 6.37 \text{ mM}$) in $\text{CF}_3\text{SO}_3\text{H}$ (pH = 1.0). Inset shows the change in absorption at 450 nm (blue diamonds + red squares).

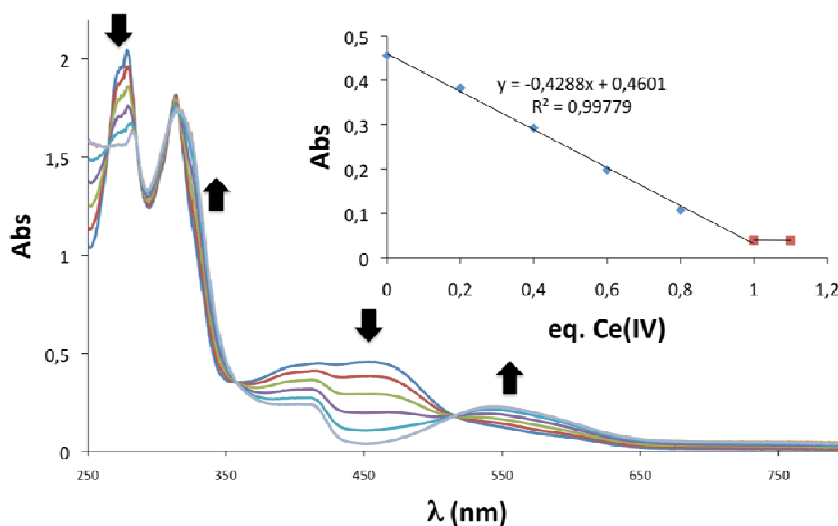


Figure S7. CV (50 mV/s) of *out-1*⁺ (dashed-dotted) and *in-1*⁺ (dotted) in DCM-TBAH (0.1 M) vs. SSCE.

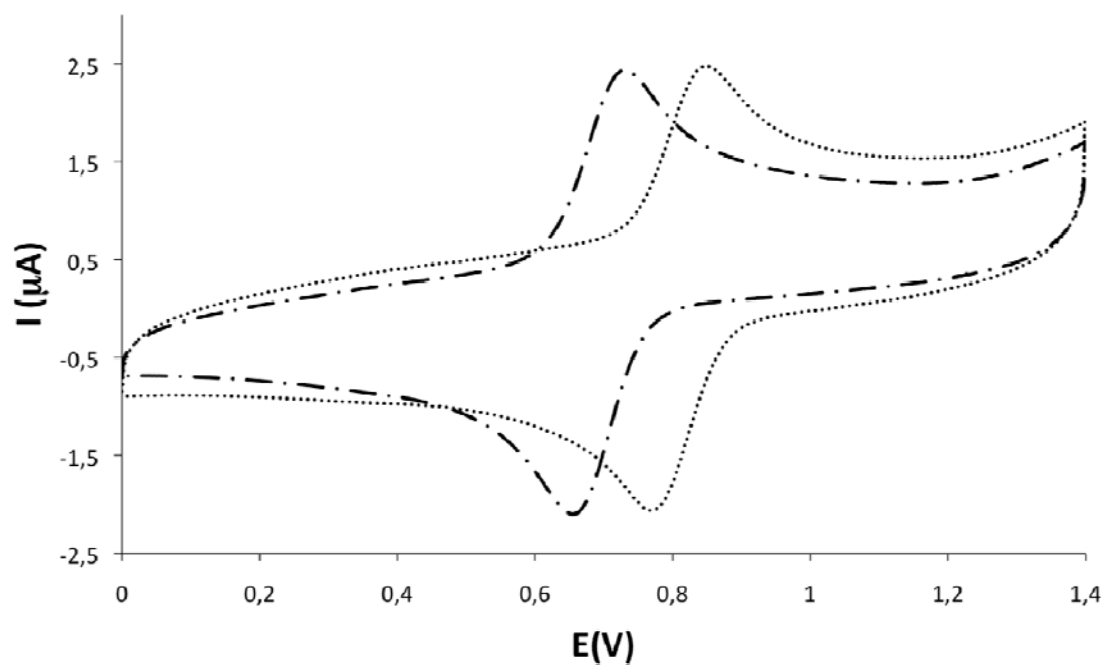


Figure S8. CV (50 mV/s) of *in-2*²⁺ (solid line) in CF₃SO₃H (pH = 1.0) vs. SSCE. Blank CV with no complex (dashed dotted line).

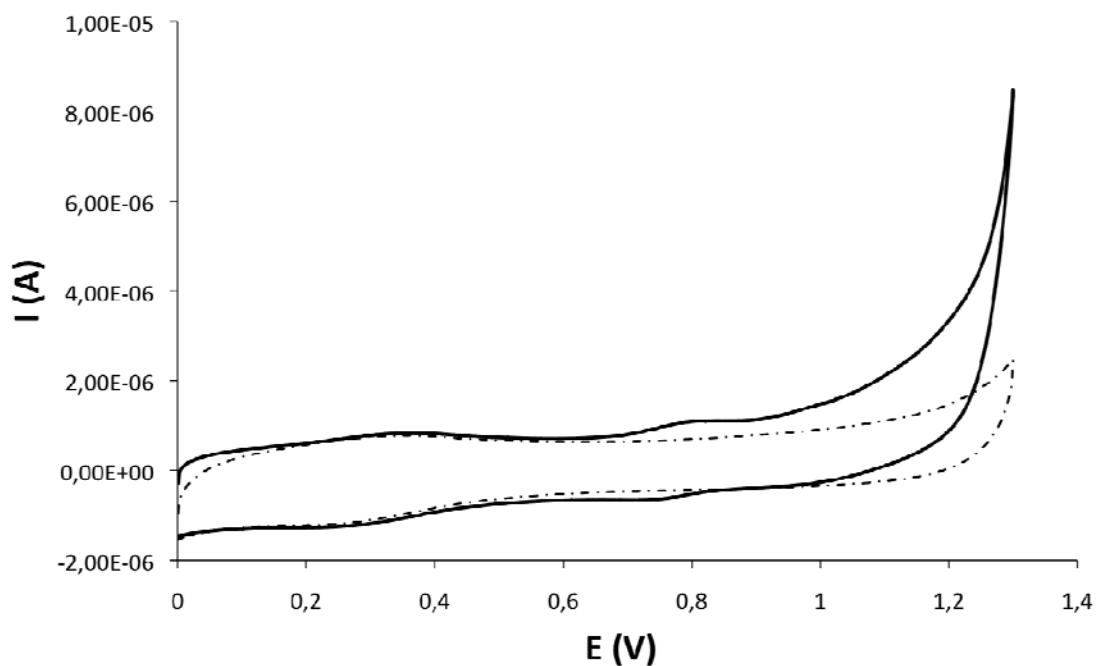


Figure S9. CV (50 mV/s) of *out-4*²⁺ (solid line and long dashed) in CF₃SO₃H (pH = 1.0) vs. SSCE. Blank CV with no complex (dashed-dotted line). SWV of *out-4*²⁺ (dotted). Inset, enlargement of the 0-1.2 V zone.

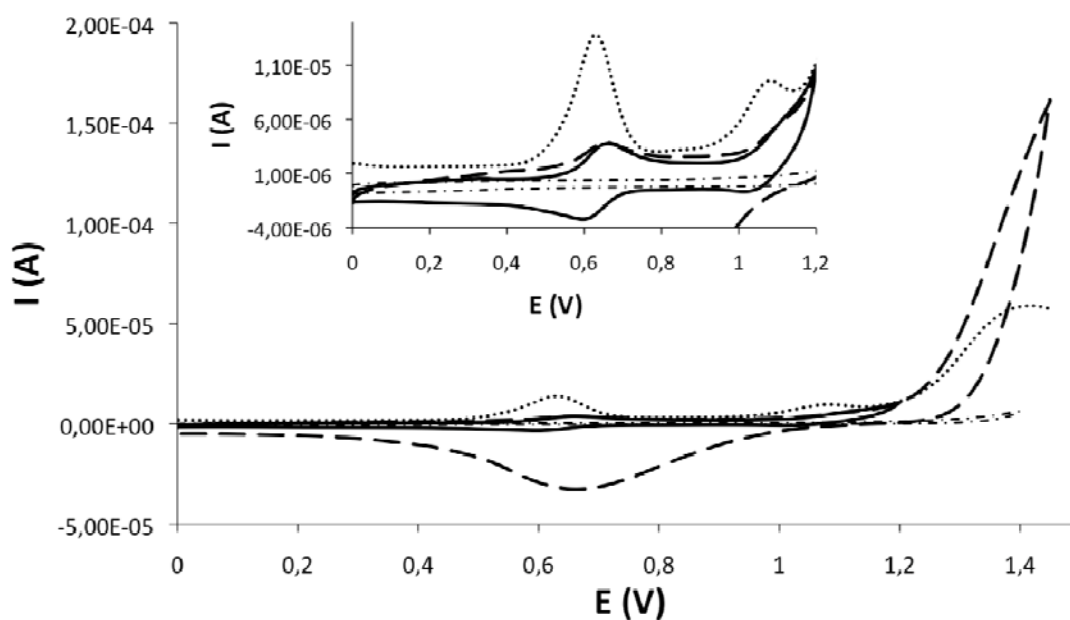


Figure S10. CV (50 mV/s) of *in-4*²⁺ (solid line and long dashed) in CF₃SO₃H (pH = 1.0) vs. SSCE. Blank CV with no complex (dashed-dotted line). SWV of *in-4*²⁺ (dotted). Inset, enlargement of the 0-1.2 V zone.

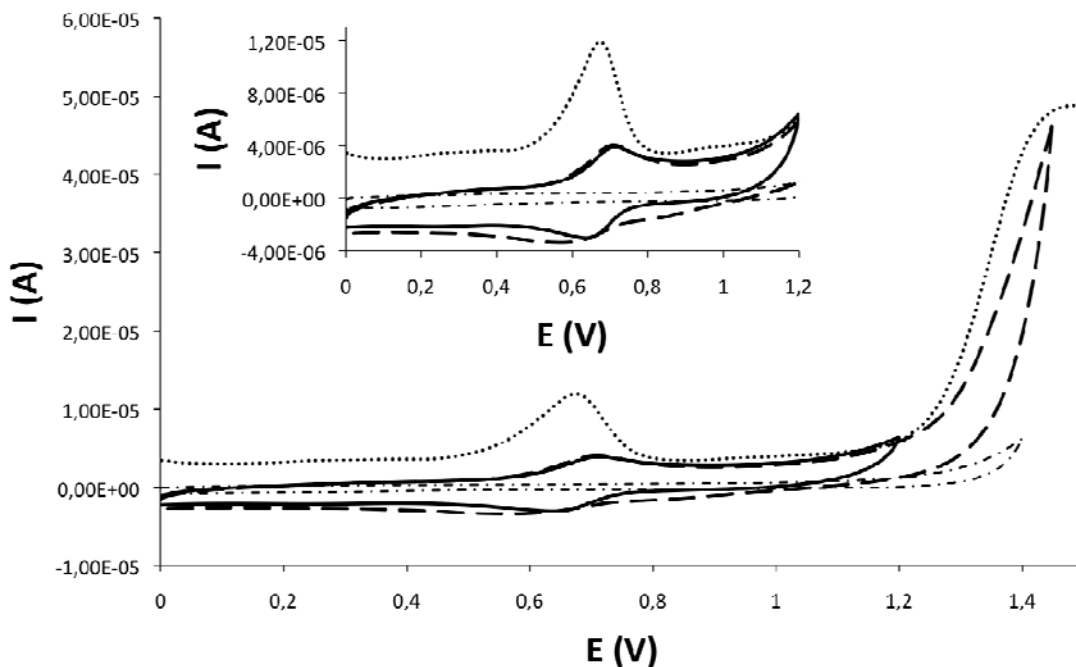


Figure S11. CV in 0.1 M triflic acid (50 mV/s) of *out-4*²⁺ (solid) and *in-4*²⁺ (dashed) under similar concentrations showing their electrocatalytic activity. CV of blank with no complex (dotted). Inset, enlargement of the 0.5-0.9 V zone.

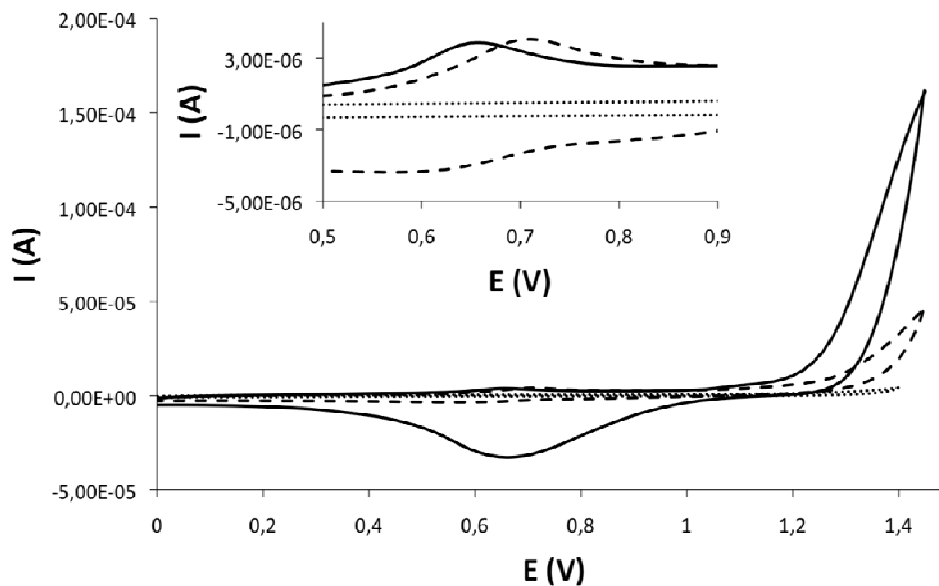
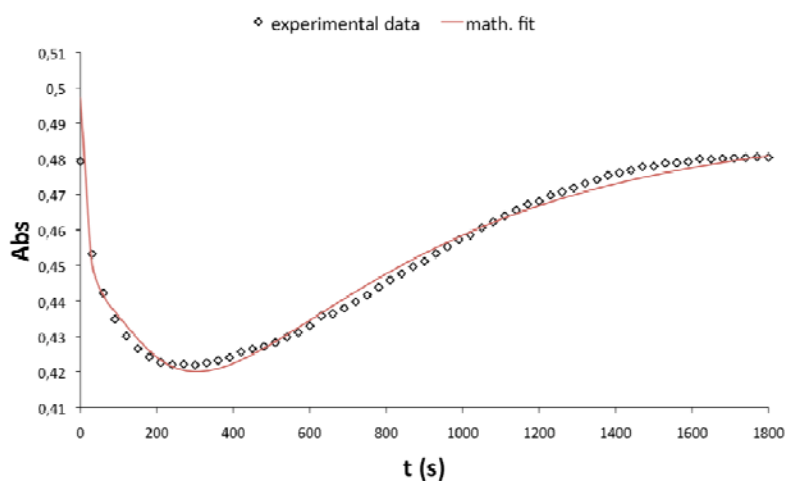
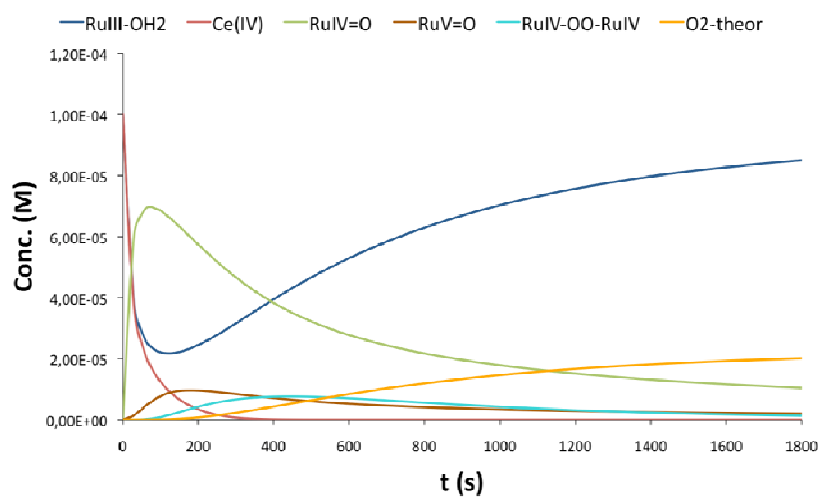


Figure S12. UV-vis spectral changes obtained upon addition of 1 equivalent of Ce(IV) to *out-4*³⁺ (Ru(III)) 0.1 mM (data recorded every 30 s). Full data presented in Figure 5 of the main text. Assuming I2M mechanism: A, absorption vs. time plot at $\lambda = 544$ nm (empty diamonds) and mathematical simulation (red solid line). B, Species distribution diagram. C, Calculated spectra. Assuming WNA mechanism. D, Species distribution diagram. E, Calculated spectra.

A



B



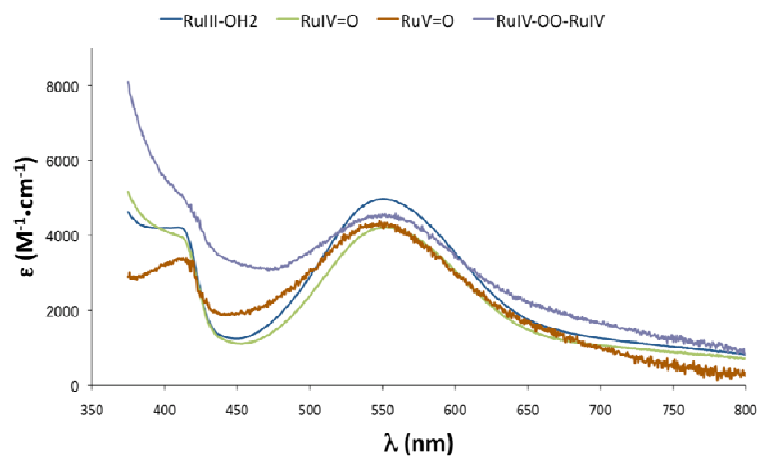
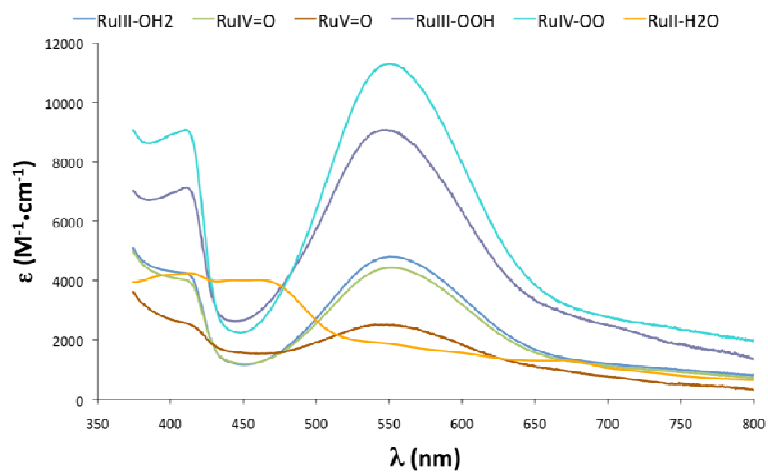
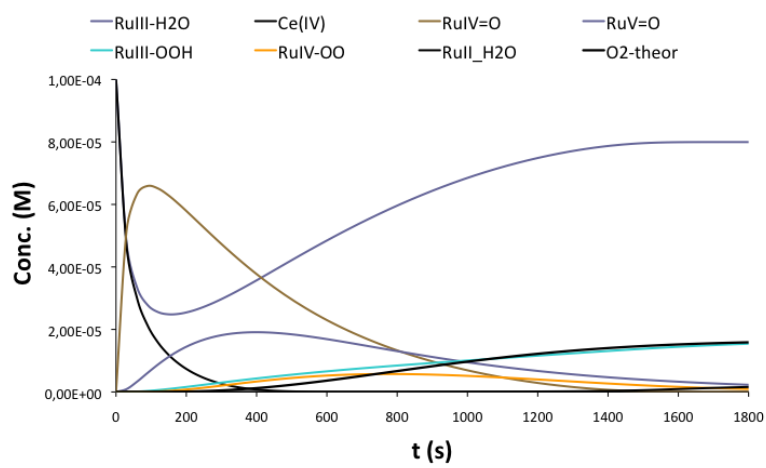
C**D****E**

Figure S13. Online mass-spectrometric analysis of the reaction of *out-2*²⁺:Ce(IV) (1:100) (left) and *in-2*²⁺:Ce(IV) (1:100) (right) in CF₃SO₃H (pH = 1.0). Arrow indicates point of injection of Ce(V).

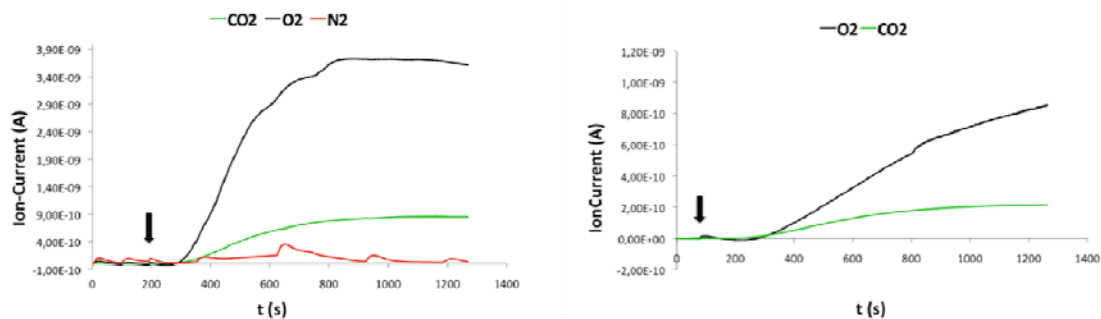


Figure S14. Online mass-spectrometric analysis of the reaction of *out-4*²⁺:Ce(IV) (1:100) (left) and *in-4*²⁺:Ce(IV) (1:100) (right) in CF₃SO₃H (pH = 1.0). Arrow indicates point of injection of Ce(V).

